

Statistical mechanics of the Huxley-Simmons model

M. Caruel^{1,*} and L. Truskinovsky²

¹*MSME, CNRS-UMR 8208, 61 Avenue du Général de Gaulle, 94010 Créteil, France*

²*LMS, CNRS-UMR 7649, Ecole Polytechnique, 91128 Palaiseau Cedex, France*

(Dated: February 12, 2022)

The chemomechanical model of Huxley and Simmons (HS) [A. F. Huxley and R. M. Simmons, *Nature* **233**, 533 (1971)] provides a paradigmatic description of mechanically induced collective conformational changes relevant in a variety of biological contexts, from muscles power-stroke and hair cell gating to integrin binding and hairpin unzipping. We develop a statistical mechanical perspective on the HS model by exploiting a formal analogy with a paramagnetic Ising model. We first study the equilibrium HS model with a finite number of elements and compute explicitly its mechanical and thermal properties. To model kinetics, we derive a master equation and solve it for several loading protocols. The developed formalism is applicable to a broad range of allosteric systems with mean-field interactions.

I. INTRODUCTION

Passive, mechanically induced conformational change in a parallel bundle of bistable elements subjected to finite temperature was first studied theoretically in the pioneering paper of A.F. Huxley and R.M. Simmons [1]. They modeled in this way the mechanism of fast force recovery in skeletal muscles subjected to shortening under a length clamp (isometric) protocol. Such loading defines a hard device ensemble, which has to be distinguished from a soft device (isotonic) ensemble exhibiting some rather different properties [2].

The HS model interpreted the conformational change, appearing in the muscle context under the name of a power stroke, in a highly simplified way, as a “digital” switch between an extended and a contracted states. HS assumed that the contracted state is biased by the imposed shortening and treated the ensuing collective folding as a deterministic chemical reaction. The information about the energetic preference of the contracted state and about the corresponding energy barriers was encoded into the reaction rates which became functions of the “mechanical configuration” of the system.

In the muscle literature the chemomechanical description of HS was later refined through the inclusion of numerous additional chemical reactions between various intermediate configurations and their kinetics was modelled phenomenologically [3–7]. Almost identical descriptions of mechanically driven conformational changes were proposed independently in the studies of cell adhesion [8, 9] and in the context of hair cell gating [10, 11]. Other closely related systems include mechanical denaturation of RNA (ribonucleic acid) and DNA (deoxyribonucleic acid) hairpins [12–14], unzipping of biological macromolecules [15–21], collective action of SNARE (soluble N-ethylmaleimide sensitive receptor) proteins during opening of synaptic pores [22] and even formation of ripples in graphene sheets [23]. For all these systems

the HS model can be viewed as a fundamental mean-field prototype.

The goal of the present paper is to reassess the chemical reaction based approach of HS from the perspective of statistical mechanics for a system with a finite number of elements while emphasizing the role of fluctuations. In such reformulation of the HS model we follow the pioneering work of T.L. Hill [3, 24] and more recent developments in Refs. [2, 25]. The zero temperature HS model was studied from this viewpoint in Ref. [26] where it was presented as a version of a fiber bundle model [27]. Here we extend the analysis of Ref. [26] to finite temperatures focusing on thermomechanical coupling that has not been previously addressed in the chemomechanical framework.

Viewed from an abstract statistical mechanics perspective, the HS model is quite similar to a paramagnetic Ising model whose thermodynamic and kinetic properties are well known [28]. The equivalence, however, is not complete due to the presence in the HS model of an elastic spring, buttressing each spin element. Another complication is the length clamp control which is unconventional for magnetic analogs of the HS system. Among the new effects revealed by the HS model, which would be unusual for paramagnets in an external field, it is enough to mention negative susceptibility and pseudo-critical behavior without genuine cooperativity.

Given that the explicit formulas for the equilibrium free energy of a spin system with mean-field interactions are rather straightforward, we can easily access both mechanical and thermal properties of the HS model including the heat release associated with mechanical loading. We can also specify the entropic contributions to mechanical and thermal susceptibilities and distinguish adiabatic from isothermal responses.

To complement the equilibrium picture, we study in this paper the stochastic dynamics of a HS system with a finite number of elements. The starting point here is a thermally induced random walk in the energy landscape biased by the mechanical loading [29, 30]. We show that due to the mean-field nature of the interactions, the kinetic properties of the HS system are fully determined

* matthieu.caruel@u-pec.fr

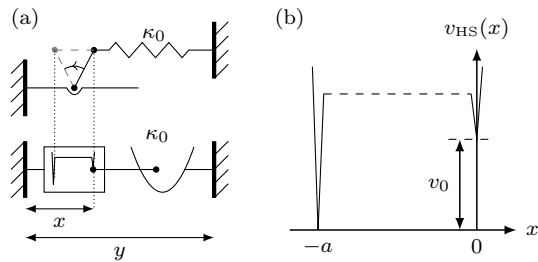


FIG. 1. Huxley-Simmons (HS) model of a single cross-bridge: (a) mechanical representation a myosin head and (b) energy landscape representing two chemical states. The conformation is characterized by the spin variable x which represents two conformations of the head. The bistable element is linked in series with a linear spring of stiffness κ_0 .

by the behavior of a single element. This justifies the approach of HS who could model the evolution of the first moment of the underlying probability distribution by a single reaction equation.

While we did not attempt in this paper to conduct a systematic quantitative comparison of our statistical HS model with experiment, we included at the end of the paper a brief discussion of the relevance of our results for skeletal muscles and for several other allosteric system with mean-field coupling.

The paper is organized as follows. In Sec. II we study the equilibrium properties of N bi stable elements connected in parallel and loaded in a hard device. Sec. III contains the analysis of the mechanical transients in this system. The applicability of the original HS model for the description of skeletal muscles is discussed in Sec. IV. Various non-muscle applications are briefly reviewed in Section V. In Sec. VI we summarize our results and identify some open problems.

II. EQUILIBRIUM

In this section we study the finite temperature equilibrium mechanical response of a folding-unfolding system containing a finite number of elements.

A. Single HS element

The Huxley-Simmons paper [1] deals essentially with a single folding element (representing a myosin cross-bridge). The HS element can be modeled as an elastic spring with stiffness κ_0 (denoted by K in Ref. [1]) which is connected in series with a bistable unit, see Fig. 1. The two states represent the two conformations of the myosin head and the variable x (denoted by $-\theta$ in Ref. [1]) takes the values 0 (pre-power-stroke or unfolded conformation) and $-a$ (post-power-stroke or folded conformation). The discrete “digital” nature of the conformational state in

the HS model allows us to interpret x as a spin variable. The soft spins (snap-springs) version of the HS model, corresponding to the case when each of the two energy wells is represented by a quadratic potential, was developed in [2, 25], however, the comparison of the two models shows that the additional effects due to elasticity of the conformational states are of mostly quantitative nature.

We choose a , denoted by h in Ref. [1], as the “reference” size of the conformational change equal to the distance between two infinitely localized energy wells, and we denote by v_0 the intrinsic energy bias distinguishing the two states; see Fig. 1. The energy of the spin element can be now written as

$$v_{\text{HS}}(x) = \begin{cases} v_0 & \text{if } x = 0, \\ 0 & \text{if } x = -a, \\ \infty & \text{otherwise.} \end{cases}$$

The energy v_0 is an implicit representation of the ATP-fueled activity in this otherwise passive system. The presence of such bias ensures that in the reference state the series spring is stretched and generates (active or tetanized) tension.

It will be convenient to use dimensionless variables and we choose a as our characteristic distance, assuming that the non-dimensional spin variable x takes values 0 or -1 . We normalize the total energy of the system by $\kappa_0 a^2$ and obtain

$$v(x; y) = (1 + x)v_0 + \frac{1}{2}(y - x)^2, \quad (1)$$

where $x = \{0, -1\}$ and y is the length of the combined element that includes a bistable unit and a linear spring. If we define $y_0 = v_0 - 1/2$ and use the muscle mechanics jargon, we can say that for $y > y_0$ (respectively $y < y_0$) the global minimum of the energy (1) corresponds to the pre-power-stroke state (respectively post-power-stroke state); in [1], the shifted elongation $y - y_0$ was denoted by y .

Note that our variable y plays a role of the external (magnetic) field for the spin variable x and therefore our model resembles the zero dimensional Ising model of paramagnetism [28]. However, due to the presence of a linear spring this Ising model is unusual: The external field has its own “energy” represented by the quadratic term in y . In the original HS experiments a muscle was loaded in a hard device which apparently makes this “energy” irrelevant. However, as we show below, the quadratic term in y brings additional stiffness into the overall mechanical response of the system and is therefore responsible for some interesting effects.

a. Thermal equilibrium. Denoting by T the absolute temperature we can write the equilibrium probability density for the configuration of a single element x at fixed y in the form

$$\rho_1(x; y, \beta) = Z_1(y, \beta)^{-1} \exp[-\beta v(x; y)], \quad (2)$$

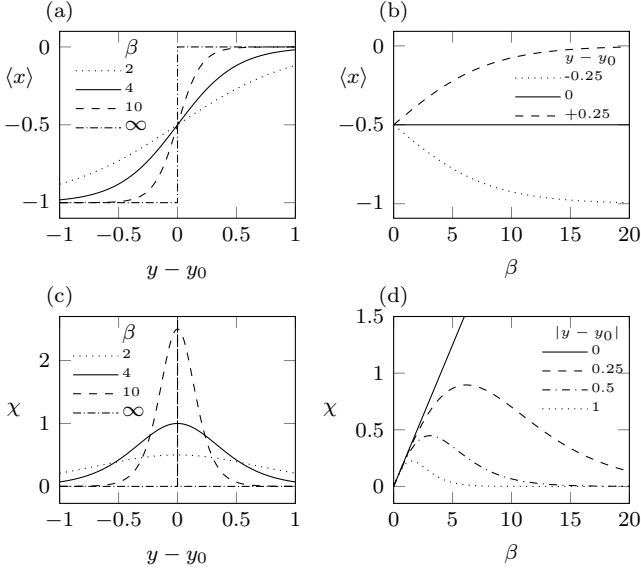


FIG. 2. Average conformation and susceptibility of a single HS element in thermal equilibrium. (a) and (b), Average configuration as a function of the applied elongation at different temperatures (a) and as a function of temperature at different elongations (b); (c) and (d), susceptibility as a function of elongation at different temperatures (c), and as function of the temperature for selected values of y (d).

where

$$\beta = \frac{\kappa_0 a^2}{k_b T}$$

is the nondimensionalized inverse temperature and k_b is the Boltzmann constant. The partition function for a single element is then

$$Z_1(y, \beta) = \exp\left[-\frac{\beta}{2}(y+1)^2\right] + \exp\left[-\beta\left(\frac{y^2}{2} + v_0\right)\right]. \quad (3)$$

From (2) we can compute the average conformation $\langle x \rangle = \sum_{x=\{0,-1\}} x \rho_1(x; y, \beta)$, obtaining,

$$\langle x \rangle(y, \beta) = -\frac{1}{2} \left\{ 1 - \tanh \left[\frac{\beta}{2} (y - y_0) \right] \right\}, \quad (4)$$

which is the analog of Eq. (15) in Ref. [1] (where the corresponding variable was denoted by $-n_2$). In paramagnetic interpretation, $\langle x \rangle(y, \beta)$ is the “average magnetization” conjugate to the “applied magnetic field” y .

The dependence of $\langle x \rangle$ on the relative elongation $y - y_0$ is illustrated in Fig. 2(a). In the zero-temperature limit the system driven through y follows the global minimum of the internal energy (1) and the population of the wells changes discontinuously at $y = y_0$ [26]. As the temperature increases, the transition smoothens and in the limit $\beta \rightarrow 0$ we have $\langle x \rangle = -1/2$ independently of the elongation as illustrated in Fig. 2(b).

By differentiating Eq. (4) with respect to y we obtain the explicit representation of the equilibrium susceptibility

$$\chi(y, \beta) = \frac{\partial}{\partial y} \langle x \rangle(y, \beta) = \beta \left\langle [x - \langle x \rangle(y, \beta)]^2 \right\rangle \quad (5)$$

which is always positive, as expected in paramagnetic systems. Given that the elastic element is linear, Eq. (5) does not depend on the particular form of the energy $v_{\text{HS}}(x)$. Thus, it also applies to models with more than two discrete states [7] and even to models with continuous energy landscape [2, 25].

Note that the susceptibility is proportional to the variance of x which in the HS model takes the form

$$\left\langle [x - \langle x \rangle(y, \beta)]^2 \right\rangle = (1/4) \left\{ \text{sech} [\beta (y - y_0) / 2] \right\}^2.$$

Both quantities will be used in what follows to assess the intensity of fluctuations.

In the zero-temperature limit the variance of x is negligible at large absolute elongations. Instead, at $y = y_0$, the strength of fluctuations is independent of temperature and we obtain that $\chi = \beta/4$, which is an analog of the Curie law in paramagnetism [28]; see Figs. 2(c) and 2(d). For other values of elongation $y \neq y_0$, one can define a characteristic temperature $\beta = \beta_\chi^*(y)$ solving the equation $\beta_\chi^*(y - y_0) \tanh [\beta_\chi^*(y - y_0)/2] = 1$. At this temperature fluctuations are maximized, see Fig. 2(d). Below the characteristic temperature the system is essentially “frozen” and therefore resistant to fluctuations. Fluctuations are also irrelevant at large temperatures where the system is maximally disordered.

b. Mechanical behavior. The free energy of a single HS element in a hard device can be computed explicitly,

$$f(y, \beta) = -\frac{1}{\beta} \log [Z_1(y, \beta)] = \frac{1}{2} y^2 + v_0 + \frac{y - y_0}{2} - \frac{1}{\beta} \ln \left\{ 2 \cosh \left[\frac{\beta}{2} (y - y_0) \right] \right\}. \quad (6)$$

Its dependence on elongation is illustrated in Fig. 3(a). We observe that for $\beta \leq 4$ (large temperatures) the free energy is convex while for $\beta > 4$ (small temperatures) it is nonconvex. The emergence of a “pseudo critical” temperature $\beta = \beta_c = 4$ in a paramagnetic system is a result of the presence of the quadratic energy associated with the “applied field” y .

To study the mechanical manifestations of the implied “criticality” we introduce the tension $\sigma = y - x$ experienced by the series linear spring. Due to the presence of the quadratic term y^2 in the energy, the conjugate variable to elongation y is not the average “magnetization” $\langle x \rangle$ but the average tension $\langle \sigma \rangle$ which is a linear function of $\langle x \rangle$ independently of the form of the potential (1).

The convexity properties of the free energy can be obtained through the study of the averaged tension-elongation relation which corresponds to Eq. (16) in

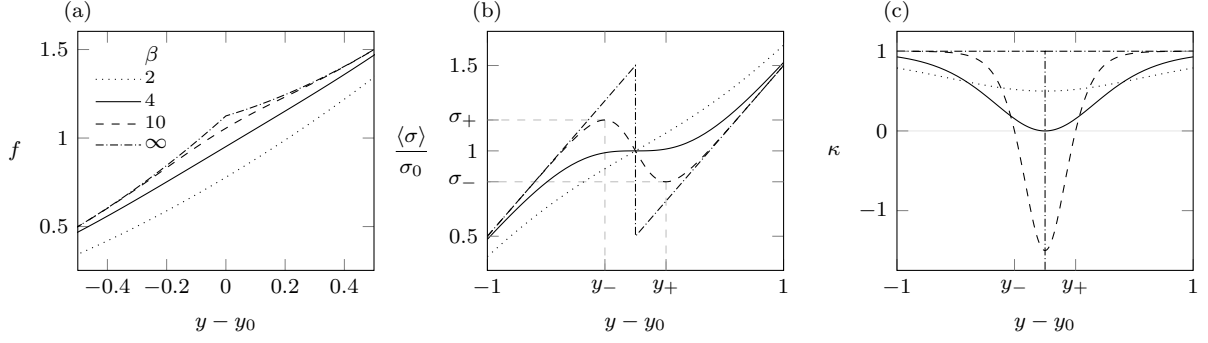


FIG. 3. Thermal equilibrium properties of the HS model in a hard device for different values of temperature. (a) Helmholtz free energy; (b) tension-elongation relations; (c) stiffness. Parameters are $\beta = 2$ (dotted), $\beta = 4$ (solid), $\beta = 10$ (dashed) and $\beta \rightarrow \infty$ (dash-dotted). In the limit $\beta \rightarrow \infty$, corresponding to zero temperature, the stiffness κ diverges at $y = y_0$, see (c).

Ref. [1],

$$\langle \sigma \rangle (y, \beta) = \frac{\partial f}{\partial y} = \sigma_0 + y - y_0 - \frac{1}{2} \tanh \left[\frac{\beta}{2} (y - y_0) \right], \quad (7)$$

where $\sigma_0 = v_0$. The dependence of $\langle \sigma \rangle$ on the elongation $y - y_0$ is illustrated in Fig. 3(b) for different values of the temperature.

We observe that while the relation $\langle x \rangle (y)$ at fixed temperature is always monotone, as it is supposed to be in a classical paramagnetic spin system, see Fig. 2, the dependence of the tension $\langle \sigma \rangle$ on its conjugate variable y can be nonmonotone, see Fig. 3(b). Behind this nonmonotonicity is the fact that the equilibrium stiffness

$$\begin{aligned} \kappa(y, \beta) &= \partial \langle \sigma \rangle (y, \beta) / \partial y = 1 - \chi(y, \beta) \\ &= 1 - \beta \left\langle [\sigma - \langle \sigma \rangle (y, \beta)]^2 \right\rangle \\ &= 1 - (\beta/4) \{ \text{sech} [\beta (y - y_0) / 2] \}^2 \end{aligned} \quad (8)$$

is a sign-indefinite sum of two terms.

Equation (8) is a representation of the standard [31, 32] decomposition of an elastic susceptibility into a Cauchy-Born part associated with affine deformation $\kappa_{\text{CB}} = 1$, and a fluctuation part associated with nonaffine deformation, here $\kappa_{\text{F}} = (\beta/4) \{ \text{sech} [\beta (y - y_0) / 2] \}^2$. Interestingly, in the HS model the fluctuation-related term in (8) does not disappear in the zero-temperature limit, producing a singular δ -function-type contribution to the affine response at $y = y_0$. At this value of the elongation the global minimum of the elastic energy is not unique and fluctuations are formally present even in the zero temperature (purely mechanical) model. This can be viewed as a manifestation of a glassy behavior [33, 34].

At finite temperatures the fluctuation-related contribution to the elastic modulus has a standard temperature dependence in pure phases $|y - y_0| \gg 1$ (softening). Instead, we observe a rubber-elasticity-type hardening type behavior around $y = y_0$, see Fig. 4. In this mixture region the negative entropic elasticity starts to dominate the positive enthalpic elasticity at $\beta > \beta_c$.

The “critical” temperature $\beta_c = 4$ is defined by the condition that the tension-elongation relation develops zero stiffness at $y = y_0$. In this state $\kappa = 1 - \beta/4$, which can be again viewed as the analog of the Curie law in magnetism. Negative stiffness, resulting from non-additivity of the system, prevails at subcritical temperatures; in this range a shortening of an element leads to a tension increase which can be interpreted as a metamaterial behavior [2, 35]. At supercritical temperatures the stiffness becomes positive, reaching asymptotically the value $\kappa = 1$.

It is remarkable that while fitting their experimental data HS found exactly the critical value $\beta = 4$ (which corresponds to the choice $4/\alpha = 8$ nm in the units adopted in Ref. [1]), concluding implicitly that the state of isometric contractions is only marginally stable. The advantages of this state are clear from Fig. 4: Small variations of temperature generate large changes in stiffness which can vary from positive to negative values and such temperature dependence is almost insensitive to the small

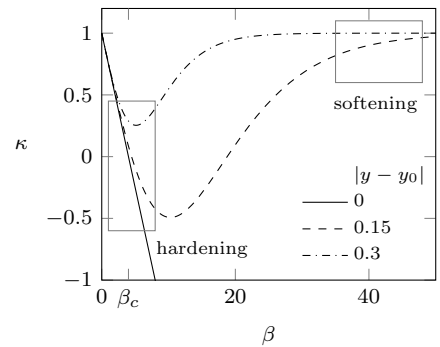


FIG. 4. Equilibrium stiffness as function of the temperature at different levels of elongation. In the low temperature regimes (large β), an increase of temperature induces softening while at high temperatures (low β) it induces hardening. Close to the critical point β_c , small changes in temperatures have a large impact on the value of the stiffness which may even change its sign.

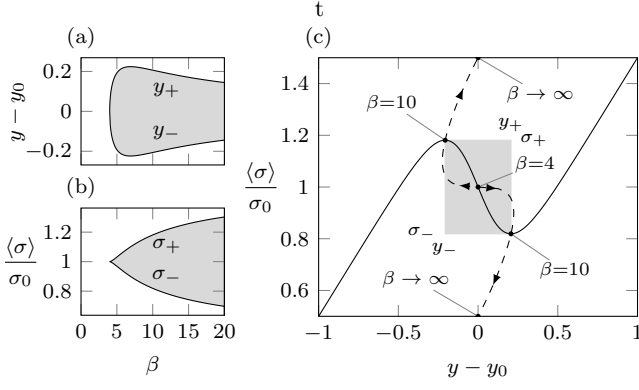


FIG. 5. The temperature dependence of the parameter domain where the HS system exhibits negative stiffness. In (a) and (b) we show the horizontal (y_+ and y_-) and vertical (σ_+ and σ_-) boundaries of the bistable domain; in (c) the dashed line is a parametric plot of $(y_-(\beta), \sigma_+(\beta))$ and $(y_+(\beta), \sigma_-(\beta))$ for ranging from $\beta = 4$ to $\beta \rightarrow \infty$. Solid line: Tension-elongation relation corresponding to $\beta = 10$ and the associated bistable domain is represented by the gray area.

changes in the stretching around y_0 . The “criticality” in HS system at y_0 , however, is subdued in the hard device ensemble, similar to the behavior of a van-der-Waals gas under controlled volume. The physical picture here is differs from the case of a ferromagnetic system under applied magnetic field where interactions and cooperativity play an important role and zero susceptibility signals the presence of a real critical point with diverging fluctuations.

To characterize the metamaterial behavior at temperatures below critical, we define an interval $[y_-, y_+]$ where the stiffness of the system is negative. The boundaries y_- and y_+ correspond to the zeros of the second derivative of the free energy. For $\beta > 4$ we have

$$y_+(\beta) - y_0 = \frac{1}{\beta} \log \left[\frac{\sqrt{\beta} + \sqrt{\beta - 4}}{\sqrt{\beta} - \sqrt{\beta - 4}} \right]$$

$$y_-(\beta) - y_0 = -\frac{1}{\beta} \log \left[\frac{\sqrt{\beta} + \sqrt{\beta - 4}}{\sqrt{\beta} - \sqrt{\beta - 4}} \right]$$

In the zero-temperature limit this interval collapses to a single point $y = y_0$. The equilibrium tensions σ_- and σ_+ corresponding to y_+ and y_- are given by

$$\sigma_+(\beta) = v_0 + \frac{1}{2} \sqrt{1 - 4\beta^{-1}} - \frac{1}{\beta} \log \left[\frac{\sqrt{\beta} + \sqrt{\beta - 4}}{\sqrt{\beta} - \sqrt{\beta - 4}} \right]$$

$$\sigma_-(\beta) = v_0 - \frac{1}{2} \sqrt{1 - 4\beta^{-1}} + \frac{1}{\beta} \log \left[\frac{\sqrt{\beta} + \sqrt{\beta - 4}}{\sqrt{\beta} - \sqrt{\beta - 4}} \right].$$

They become equal to $\sigma_+ = v_0 + 1/2$ and to $\sigma_- = v_0 - 1/2$, when $\beta \rightarrow \infty$, see Ref. [26] for more detail. The evolution of the domain of metamaterial behavior with temperature is shown in Fig. 5.

We finish this subsection with the observation that since $\langle \sigma \rangle(y, \beta) = y - \langle x \rangle(y, \beta)$, we have

$\langle [\sigma - \langle \sigma \rangle(y, \beta)]^2 \rangle = \langle [x - \langle x \rangle(y, \beta)]^2 \rangle$, which shows that the fluctuations of tension originate from the fluctuations of the conformation. In this sense the “noisy” macroscopic force-elongation relations can be used as an experimental window into the microscopic behavior of the system.

c. Thermal behavior. While the experiments on muscles have been traditionally focused on the mechanical response [36–43], our study suggests that measuring the thermal or calorimetric response of such systems may be at least as informative, see some existing work along these lines on muscles in Refs. [44–50]. The statistical HS model has a considerable predictive power in this respect. For instance, the entropy of the HS element can be computed explicitly,

$$s(y, \beta) = -\beta \frac{\partial}{\partial \beta} \log [Z_1(y, \beta)] + \log [Z_1(y, \beta)]$$

$$= \log \left\{ 2 \cosh \left[\frac{\beta}{2} (y - y_0) \right] \right\}$$

$$- \frac{\beta}{2} (y - y_0) \tanh \left[\frac{\beta}{2} (y - y_0) \right]. \quad (9)$$

and we illustrate the behavior of the function $s(y, \beta)$ in Figs. 6(a) and 6(b). We see that the degree of disorder is maximal in the state of isometric contractions, $y = y_0$. Note also that the entropy depends on a single normalized coordinate $\beta (y - y_0)$ combining both control parameters, temperature and displacement.

A measure of the dependence of the entropy on tem-

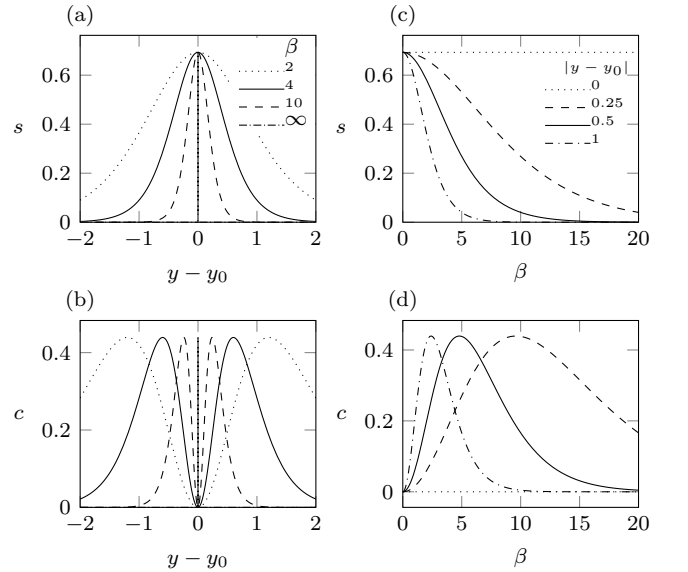


FIG. 6. Entropy [(a) and (b)] and specific heat [(c) and (d)] in thermal equilibrium represented as function of elongation at different temperatures [(a) and (d)] and as function of temperature for different elongations [(b) and (d)].

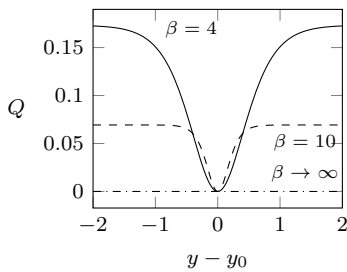


FIG. 7. Isothermal heat released induced by a displacement from the state $y = y_0$ at different temperatures.

perature is the specific heat [28]

$$c(y, \beta) = -\beta \frac{\partial}{\partial \beta} s(y, \beta) = \left\{ \frac{\beta}{2} (y - y_0) \operatorname{sech} \left[\frac{\beta}{2} (y - y_0) \right] \right\}^2,$$

which is represented as function of $y - y_0$ and β in Figs. 6(c) and 6(d). As is typical for paramagnetic systems, the specific heat depends only on the combination $\beta(y - y_0)$. Since at $y = y_0$, the entropy is temperature insensitive [$s(y_0) = \log(2)$], the specific heat vanishes. Similarly, at large elongations, the system becomes more and more ordered and temperature changes no longer affect the entropy. As a result, the specific heat is maximized at a characteristic value of the temperature $\beta = \beta_c^*$ which solves the equation $\beta_c^*(y - y_0) \tanh[\beta_c^*(y - y_0)/2] = 2$.

To study the heat release associated with the change of length we can use our knowledge of the entropy variation with y . We introduce the heat release $Q(y, \beta) = -\beta^{-1} \Delta s(y, \beta)$, where $\Delta s(y, \beta) = s(y, \beta) - s(y_{in}, \beta)$, is the entropy change from the initial state y_{in} . The function Q , which is illustrated in Fig. 7, can be potentially measured by calorimetric techniques if the system is first driven away from equilibrium adiabatically by a rapid length change and then allowed to relax reaching the original temperature.

Note that the expression for entropy (9) can be also rewritten in the form $s = \beta \langle v \rangle - \beta f$ where $\langle v \rangle$ is the

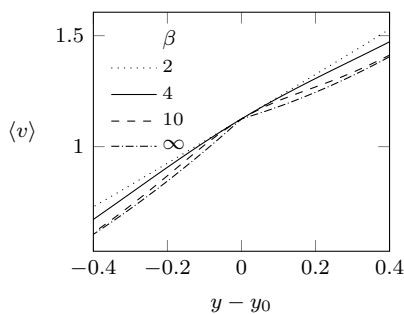


FIG. 8. Average internal energy for $\beta = 2$ (dotted), $\beta = 4$ (solid), $\beta = 10$ (dashed) and in the athermal limit $\beta \rightarrow \infty$ (dot-dashed).

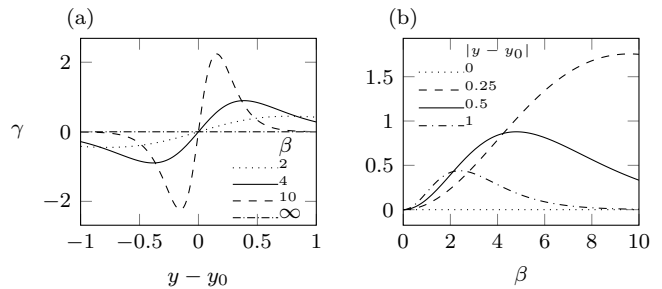


FIG. 9. The dependence of the coefficient γ on elongation (a) and temperature (b).

average internal energy

$$\langle v \rangle(y, \beta) = y^2/2 + v_0 - (y - y_0) \langle x \rangle(y, \beta).$$

In contrast to the equilibrium free energy, which decreases with temperature, see Fig. 3(a), the average internal energy increases with temperature, see Fig. 8. In the opposite zero temperature (athermal) limit ($\beta \rightarrow \infty$) both the average internal energy and the free energy tend to the same limiting curve representing the global minimum of the elastic energy which is a nonconvex function of elongation energy [26]. Observe, however, that the average internal energy approaches the mechanical energy “from above” while the free energy approaches the mechanical energy “from below”.

Another interesting and potentially measurable quantity is the entropic contribution to stress which also serves as a measure of thermal expansion

$$\gamma = -\frac{\partial s}{\partial y} = \frac{\beta^2}{4} (y - y_0) \left\{ \operatorname{sech} \left[\frac{\beta}{2} (y - y_0) \right] \right\}^2.$$

The dependence of γ on elongation and temperature is illustrated in Fig. 9. We observe that for $y > y_0$ (respectively $y < y_0$) the growth of temperature enhances (respectively diminishes) the tension, see Fig. 3(b), and the temperature sensitivity of tension is the highest at a particular value of the temperature. In large shortening or stretching regimes and at $y = y_0$, the mechanical response is temperature insensitive.

d. Adiabatic response. The knowledge of the thermal properties of the HS model allows one to address the question of whether the isothermal approximation is justified when applied to experiments involving folding or unfolding under fast loading. Below, we consider an alternative hypothesis that the response is adiabatic, which implies that in this problem the heat exchange is the rate-limiting process. To remain within the equilibrium framework, we replace the task of computing the actual adiabats by computing the isoentropes to which we will be still referring as adiabats. We discuss the applicability of the adiabatic assumption for the description of fast force recovery in muscles in Sec. IV.

As the entropy of the system depends solely on $\beta|y - y_0|$, see Eq. (9), the temperature varies along the adiabats

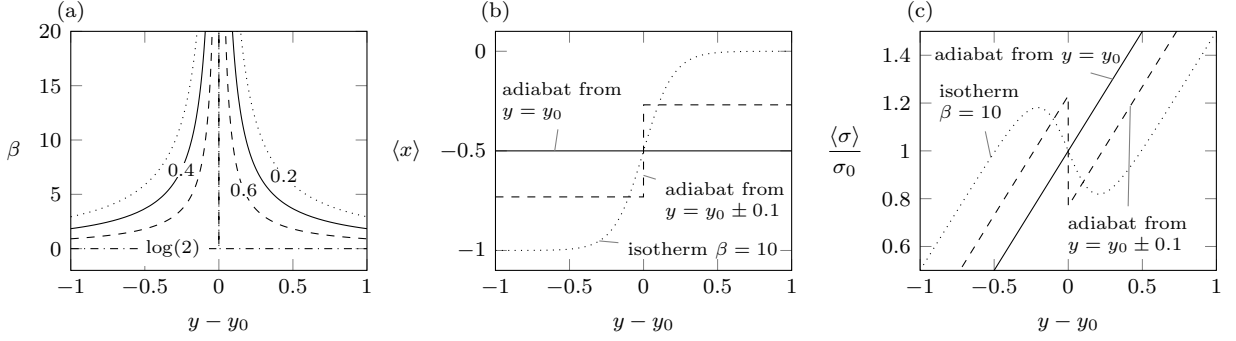


FIG. 10. Adiabatic response. (a) Evolution of temperature as function of the applied loading along adiabats for $s = 0.2$ (dotted), $s = 0.4$ (solid), and $s = 0.6$ (dashed). (b) Average conformation following adiabatic length changes from two different thermal equilibrium initial conditions $y = y_0$ (solid) and from $y = y_0 \pm 0.1$ (dashed) at $\beta_{\text{in}} = 10$. The isothermal response is represented by the dotted line. (c) Adiabatic tension-elongation relations. Dotted line, isotherm response for $\beta = 10$; dashed line, adiabatic response with initial state at $y - y_0 = \pm 0.1$ with $\beta_{\text{in}} = 10$; solid line, adiabatic response with initial state at $y = y_0$ with $\beta_{\text{in}} = 10$.

proportionally to the elongation, see Fig. 10(a). More specifically, along an adiabat starting at $y = y_{\text{in}}$ with temperature $\beta = \beta_{\text{in}}$, we have $\beta_{\text{ad}} = \beta_{\text{in}} \frac{|y_{\text{in}} - y_0|}{|y - y_0|}$. Since, according to Eq. (4), the average configuration depends only on $\beta(y - y_0)$, the variation of temperature along adiabats must ensure that the average configuration $\langle x \rangle$ is preserved. This is true for every value of y except $y = y_0$ where the adiabat experiences a discontinuity. Along adiabats the average configuration evolves according to

$$\langle x \rangle_{\text{ad}}(y, \beta) = -\frac{1}{2} + \frac{1}{2} \tanh \left[\frac{\beta_{\text{in}} |y_{\text{in}} - y_0|}{2} \text{sign}(y - y_0) \right].$$

The adiabatic response of the microconfiguration of the system to abrupt “length steps” is illustrated in Fig. 10(b), where the initial temperature is always $\beta_{\text{in}} = 10$. Observe that for the adiabat passing through the point $y = y_0$ the average configuration is frozen at $\langle x \rangle = -1/2$ (solid line); the behavior of a microconfiguration along an *isotherm* passing through $y = y_0$ drastically differs (dotted line).

Since equilibrium tension along the adiabats depends linearly on $\langle x \rangle$, the adiabatic stress response to shortening from $y = y_0$ is quasilinear elastic, even though the temperature is changing. More specifically, one can show that outside the point $y = y_0$ the adiabatic stiffness is equal to the purely mechanical stiffness

$$\kappa_{\text{ad}} = \frac{\partial^2}{\partial y^2} f(y, \beta_{\text{ad}}(y, s)) = \kappa_0 \geq \kappa,$$

where the function $\beta_{\text{ad}}(y, s)$ describes temperature variation with elongation at a given entropy s .

Note that at $y = y_0$, the inverse temperature β diverges and even small adiabatic length change would lead to a dramatic increase of temperature ($\beta \rightarrow 0$). This means, in particular, that reaching this state adiabatically brings about infinite cooling. A similar effect in a paramagnetic spin system is known as “cooling by adiabatic demagnetization.” In the HS system the applied field $y - y_0$ can

be both positive and negative and, in this case, if $y < y_0$, a shortening would lead to a similar “adiabatic heating,” which can be, in principle, measured in experiment, see Section IV.

For the adiabats starting at other points $y \neq y_0$ the average configuration $\langle x \rangle$ is frozen at its initial value until the loading reaches the point $y = y_0$. At this point the continuity of entropy requires that the configuration changes discontinuously. Due to adiabatic cooling at $y - y_0$ the temperature goes to zero and the response becomes discontinuous (quasimechanical, see [26]). This is in stark contrast with continuous evolution of the configuration along a typical isotherm also shown in Fig. 10(b) (dotted line). One can say that, during adiabatic response, the temperature-induced smoothing of the force-elongation relation gets overridden by the anomalous cooling around the point $y = y_0$.

The adiabatic tension-elongation relations originating from this behavior of the microconfiguration are piecewise linear with stiffness equal to 1 for $y \neq y_0$, see Fig. 10(c). The presence of a discontinuity at $y = y_0$ signifies an extreme metamaterial-type behavior. Interestingly, the adiabat originating exactly from the equilibrium state $y = y_0$ can be confused with the purely elastic isothermal force elongation relation. The associated temperature variation, however, is non-negligible and should be, in principle, measurable in experiments.

B. Bundle of HS elements

Consider now a finite number of HS elements attached in parallel between two rigid backbones. In the skeletal muscle context, such a bundle represents a minimal actomyosin complex which we refer to as an elementary half-sarcomere, see Fig. 11.

The energy of the system with N elements can be writ-

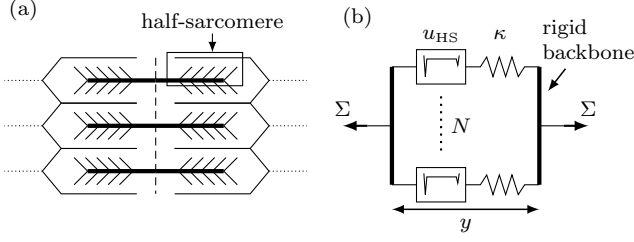


FIG. 11. (a) Schematic representation of an acto-myosin filaments organization in a superstructure of half-sarcomeres. (b) A single half-sarcomere represented as a cluster containing N cross-linkers, see Fig. 1. The control parameter is the total elongation y and the total tension generated by the system is denoted by Σ .

ten as

$$e(\mathbf{x}; y) = \frac{1}{N} \sum_{i=1}^N \left[(1 + x_i) v_0 + \frac{1}{2} (y - x_i)^2 \right],$$

where $\mathbf{x} = \{x_1, \dots, x_N\}$. The individual bistable elements do not interact among themselves while they all interact with the same external field y . The origin of this mean-field type interaction is a hard device constraint which is not affected by the microconfiguration of the system. In the language of magnetism, we are dealing here with a one-dimensional paramagnetic system. In fact, for such systems, the dimensionality is irrelevant and one can expect the results obtained for the zero-dimensional model to remain valid for the case of N elements.

e. Thermal equilibrium. In thermal equilibrium, the probability density for a micro-state \mathbf{x} reads

$$\rho(\mathbf{x}; y, \beta) = Z(y, \beta)^{-1} \exp[-\beta e(\mathbf{x}; y)], \quad (10)$$

where the partition function is

$$Z(y, \beta) = \sum_{\mathbf{x} \in \{0, -1\}^N} \exp[-\beta N e(\mathbf{x}; y)].$$

Due to the additivity of the energy we obtain $Z(y, \beta) = [Z_1(y, \beta)]^N$, where Z_1 is given by (3). Therefore $\rho(\mathbf{x}; y, \beta) = \prod_{i=1}^N \rho_1(x_i; y, \beta)$ which shows that the elements are independent.

The total free energy can be written as $F(y, \beta) = N f(y, \beta)$, where the expression for the free energy of a single HS element f is given by (6); this formula is analogous to the corresponding result for paramagnetic Ising model and other mean-field-type systems, e.g., Ref. [16]. Similarly, other extensive equilibrium variables are also additive and it will be convenient to normalize them by N .

To shed light on the internal *microconfiguration* of the system we introduce the fraction of HS elements in the folded conformation

$$p = -\frac{1}{N} \sum_{i=1}^N x_i,$$

which, in our case, plays the role of an order parameter. The internal energy (per element) corresponding to a given p can be written as

$$e(p, y) = p(y+1)^2/2 + (1-p)(y^2/2 + v_0). \quad (11)$$

Due to permutational invariance, we can write the probability of a given state with Np elements in the folded state in the form of the binomial law:

$$\rho(p; y, \beta) = \binom{N}{Np} [\rho_1(-1; y, \beta)]^{Np} [\rho_1(0; y, \beta)]^{N(1-p)}, \quad (12)$$

where ρ_1 is given by (2) and $\rho_1(0; y, \beta) = 1 - \rho_1(-1; y, \beta)$.

Note that the distribution (12) can be also written as

$$\rho(p; y, \beta) = Z(y, \beta)^{-1} \exp[-\beta N \tilde{f}(p; y, \beta)]$$

where

$$\tilde{f}(p; y, \beta) = e(y, p) - (1/\beta) s(p), \quad (13)$$

is the marginal free energy, e is the internal energy (11), and $s(p) = \frac{1}{N} \log \binom{N}{Np}$ is the ideal entropy, all corresponding to a fixed value of p and finite N .

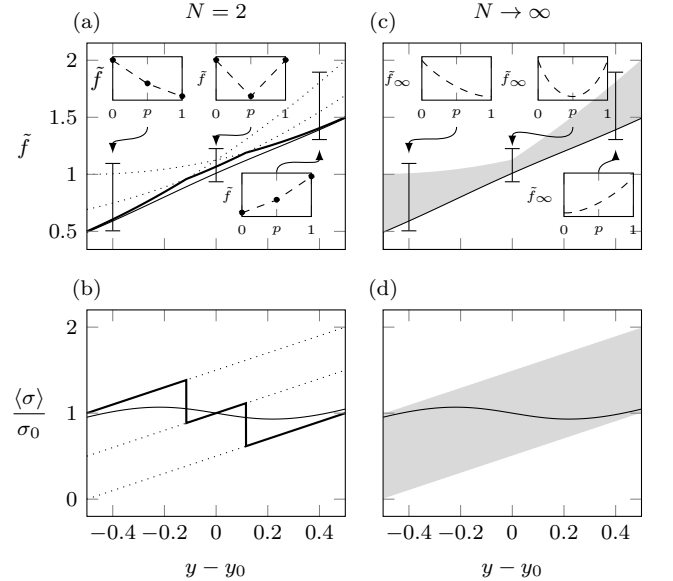


FIG. 12. Nonequilibrium free energy landscape and the corresponding tension-elongation relations in a hard device for $N = 2$ [(a) and (b)] and in the limit $N \rightarrow \infty$ [(c) and (d)]. Dotted lines, free-energy levels, and tension corresponding to different values of p ; thick line, response corresponding to the global minimum of the nonequilibrium free energy; thin lines, response in thermal equilibrium; gray areas, domain of the metastable states in the thermodynamic limit. In (a) and (c), the inserts show the marginal free energy \tilde{f} as function of p for $y - y_0 = -0.4, 0, 0.4$. The plots are obtained with $\beta = 6$, which explains the presence of negative stiffness.

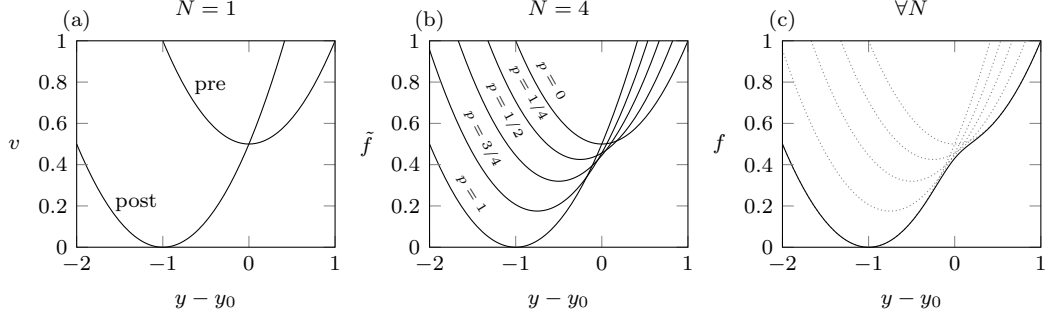


FIG. 13. Hill-type energy landscapes for $N = 1$ (a) and $N = 4$ (b). In (c) we show the equilibrium free-energy profile $f = F/N$ (solid line), which is independent of N together with the metastable states for $N = 4$ (dotted lines). Here $v_0 = 1/2$.

To illustrate Eq. (13), consider the simplest case $N = 2$ when the marginal free energy can take only three values,

$$\begin{aligned}\tilde{f}(0; y, \beta) &= e(0; y) = \frac{1}{2}y^2 + v_0 \\ \tilde{f}(1/2; y, \beta) &= \frac{1}{4}(y+1)^2 + \frac{1}{4}y^2 + \frac{1}{2}v_0 - \frac{\log(2)}{2\beta} \\ \tilde{f}(1; y, \beta) &= e(1; y) = \frac{1}{2}(y+1)^2,\end{aligned}$$

which are shown in Fig. 12 together with the corresponding tension-elongation relations. Observe that the global minimum response at finite temperature is characterized by a series of *jumps* reflecting successive conformational changes in individual elements. Between the jumps, the stiffness is positive, which shows that each metastable state has a finite basin of stability even though the overall (global) stiffness is negative.

The changes in the marginal free-energy profiles with increasing N are illustrated in Fig. 13. At $N = 1$, we obtain the representation of the energy landscape due to T. L. Hill [36]. In this case, the marginal free energy \tilde{f} and the internal energy v are identical (no entropic contribution). For finite N we obtain $N + 1$ metastable states corresponding to different values of p with the global minimum represented by a (nonconvex) lower envelope.

While the lower envelope of the marginal free energy $\tilde{f}(y, \beta) = \min_p \tilde{f}(p, y, \beta)$ is a piecewise smooth function of y with a number of singular points depending on N , the equilibrium free energy $f(y, \beta) = F(y, \beta)/N$ is a smooth function laying strictly below: $f(y, \beta) \leq \tilde{f}(y, \beta)$. The N independence of $f(y, \beta)$ —see Eq. (6)—shows that for the HS system the equilibrium response is size independent. However, in real experiments for systems with small N conducted at finite deformation rates one can expect to see the steps on the force elongation curves associated with the singularities of $\tilde{f}(y)$, see Sec. III B.

The average value of the parameter p (which is analogous to the variable n_2 in Ref. [1]) can be found from

$$\langle p \rangle(y, \beta) = \sum p \rho(p; y, \beta) = -\langle x \rangle(y, \beta) = \rho_1(-1; y, \beta) \quad (14)$$

This quantity plays the role of the average magnetization per spin and does not depend on N ; however, the corresponding variance decreases as $1/N$,

$$\langle [p - \langle p \rangle(y, \beta)]^2 \rangle = (1/N) \langle [x - \langle x \rangle(y, \beta)]^2 \rangle.$$

Our Eq. (14) also shows that the whole distribution (12) can be recovered if the parameter N is fixed and $\langle p \rangle$ is known as a function of y and β . In particular, we can compute the variance

$$\langle [p - \langle p \rangle(y, \beta)]^2 \rangle = \langle p \rangle(1 - \langle p \rangle), \quad (15)$$

which gives after substitution

$$\langle [p - \langle p \rangle(y, \beta)]^2 \rangle^{1/2} = \frac{1}{2\sqrt{N}} \text{sech} \left[\frac{\beta}{2}(y - y_0) \right]. \quad (16)$$

By differentiating Eq. (14) with respect to y we can also obtain the equilibrium susceptibility

$$X(y, \beta) = -\frac{\partial}{\partial y} \langle p \rangle = \beta N \langle (p - \langle p \rangle)^2 \rangle = \chi(y, \beta),$$

where χ is the susceptibility of a single HS element, see Eq. (5). We can similarly rewrite all other equilibrium characteristics of the system in terms of $-\langle p \rangle$ and $N \langle [p - \langle p \rangle(y, \beta)]^2 \rangle$.

In the limit $N \rightarrow \infty$ the expression for the marginal free energy can be written explicitly

$$\tilde{f}_\infty(p; y, \beta) = e(p; y) - (1/\beta) s_\infty(p), \quad (17)$$

where $s_\infty(p) = -[p \log(p) + (1-p) \log(1-p)]$, is the ideal mixing entropy reflecting the absence of correlations between the units. The function $\tilde{f}_\infty(p)$ is always convex since

$$\frac{\partial^2}{\partial p^2} \tilde{f}_\infty(p; y, \beta) = [\beta p(1-p)]^{-1} > 0,$$

which signifies the lack of synchronization: In a similar ferromagnetic system the marginal free energy would be nonconvex. As $N \rightarrow \infty$ the domain of the phase space occupied by the metastable states becomes compact, see

the gray area in Figs. 12(c) and 12(d) not shown explicitly in Fig. 13(c).

At large N , the summation over the set of discrete values of p (see Eq. (14)) can be approximated by an integration over the interval $[0, 1]$. The integrals can be, in turn, computed by using the Laplace method. Then, for the equilibrium free energy, we can write $f(y, \beta) = \tilde{f}_\infty(p_*(y, \beta); \beta)$, where f and \tilde{f}_∞ are given by (6) and (17), respectively. Here $p_*(y, \beta)$ is a minimizer of \tilde{f}_∞ , which is a solution of the transcendental equation,

$$p_*/(1 - p_*) = \exp[-\beta(y - y_0)].$$

It is easy to check that $p_*(y, \beta) = \langle p \rangle(y, \beta)$ where $\langle p \rangle(y, \beta)$ is given by Eq. (14). The resulting free-energy profile is shown in both Fig. 12(c) and Fig. 13(c).

f. Mechanical behavior. For a given configuration \mathbf{x} , the tension in the system can be written as

$$\Sigma(\mathbf{x}, y) = N \left[y - (1/N) \sum x_i \right] = N(y + p).$$

The average tension, conjugate to the control parameter y , is then

$$\langle \Sigma \rangle(y, \beta) = N[y + \langle p \rangle(y, \beta)] = N\langle \sigma \rangle(y, \beta),$$

where $\langle \sigma \rangle$ is the average tension of a single element, see Eq. (7). The variance of the total tension can be written as

$$\langle [\Sigma - \langle \Sigma \rangle(y, \beta)]^2 \rangle = N \langle [\sigma - \langle \sigma \rangle(y, \beta)]^2 \rangle.$$

The relative fluctuations,

$$\frac{\langle [\Sigma - \langle \Sigma \rangle(y, \beta)]^2 \rangle^{1/2}}{\langle \Sigma(y, \beta) \rangle} = \frac{1}{2\sqrt{N}} \left\{ \left(y + \frac{1}{2} \right) \cosh \left[\frac{\beta}{2}(y - y_0) \right] - \frac{1}{2} \sinh \left[\frac{\beta}{2}(y - y_0) \right] \right\}^{-1} \quad (18)$$

decay as $1/N^{1/2}$, which is a sign that the measured force in this model is an extensive quantity. The formula (18) can be used to estimate the number of elements N from the knowledge of the fluctuations of the force.

If we denote by K the total stiffness of the system, then we can write

$$K(y, \beta) = N\kappa(y, \beta) = N - \beta \langle [\Sigma - \langle \Sigma \rangle(y, \beta)]^2 \rangle \quad (19)$$

where κ is defined by Eq. (8). As in the case of a single HS element, the total stiffness decomposes into an elastic (or enthalpic) contribution dominating at $|y - y_0| \gg 1$ and a term containing entropic contribution which dominates around $y = y_0$.

In dimensional form (19) becomes

$$\begin{aligned} K^d &= N\kappa_0 - \frac{1}{k_b T} \langle [\Sigma^d - \langle \Sigma \rangle^d]^2 \rangle \\ &= N\kappa_0 \left[1 - \frac{\kappa_0 a^2}{4k_b T} \left\{ \text{sech} \left[\frac{\kappa_0 a}{2k_b T} (y^d - y_0^d) \right] \right\}^2 \right], \end{aligned} \quad (20)$$

where the superscript d indicates that the normalization has been dropped.

Note, first, that the fluctuation-related contribution to stiffness is an order of one effect in terms of the number of elements N , which means that the effect of fluctuations does not disappear in the thermodynamic limit. Also, since the stiffness in the HS model is an extensive property, the analysis of the temperature and elongation dependence of $\kappa(y, \beta)$ presented in Sec. II A remains valid here as well.

The fact that the stiffness has an nonthermal, purely mechanical part, that can be potentially extracted from structural measurements, and an equally important and even dominating fluctuation-related component, that can be measured independently, has been largely overlooked in the literature on systems with nonconvex internal degrees of freedom because in classical materials, which can be thought to be composed of almost linear springs, the fluctuational effect on stiffness is usually small. Here we see that in the presence of internal “snap-springs” this effect can be considerable. For instance, the difference between the smaller quasistatic stiffness of myosin II [51, 52] and the larger instantaneous stiffness—believed to be largely unaffected by fluctuations [53]—may be linked to the importance of the second term in our Eq. (20).

On the other hand, if N is known and the variance of the total force can be measured, then one can recover the stiffness of a single element κ_0 . Conversely, knowing κ_0 and measuring fluctuations of the force one can estimate N from (20). We emphasize again that the relation (20) is independent of the detailed structure of the energy landscape (1) and can therefore be used in the presence of multiple power-stroke-type energy wells.

g. Thermal behavior. Since the entropy of the finite size bundle of HS elements is extensive $S(y, \beta) = Ns(y, \beta)$, the analysis of the adiabatic response for a single HS element presented in Sec. II A remains valid for the bundle of N HS elements.

III. KINETICS

In this section we study kinetics of the HS system and build links between the stochastic dynamics of a single HS element, the evolution of the bundle of HS elements connected in parallel, and a conventional chemomechanical modeling of such systems in terms of deterministic chemical reactions. Following the original HS model, we assume for simplicity that during loading the temperature is kept constant.

A. Single HS element

In the paper of Huxley and Simmons [1] the relaxation of the system to equilibrium was modeled as a deterministic chemical reaction of the first order. In their description HS followed the average population of elements

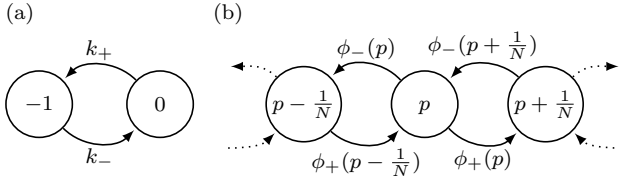


FIG. 14. One-dimensional Markov chain description for a single HS element (a) and for a system with N elements (b).

in the two conformational states without attempting to trace the dynamics of individual flips experienced by the spin variables x .

To simulate stochastic dynamics of a single HS element we need to know the probabilities of the forward and reverse flips

$$\begin{aligned} \mathbb{P}[x^{t+dt} = -1 | x^t = 0] &= k_+(y, \beta) dt \\ \mathbb{P}[x^{t+dt} = 0 | x^t = -1] &= k_-(y, \beta) dt. \end{aligned} \quad (21)$$

Here $k_+(y, \beta)$ [respectively $k_-(y, \beta)$] is the transition rate for the jump from the unfolded state (respectively, folded state) to the folded state (respectively, unfolded state), see Fig. 14(a). We assume that the total elongation y and the inverse temperature β are the controlling parameters which may vary at a time scale much larger than the characteristic time of the individual conformational transitions. As the transition probabilities (21) depend only on the current state of the system, the dynamics is described by a discrete Markov chain [30, 54].

To compute the transition rates $k_{\pm}(y, \beta)$ we need to know the structure of the actual energy landscape separating the two conformational states. In their paper [1], HS simply assumed that the hypothetical barrier sepa-

rating the two wells of the potential v_{HS} is flat and is characterized by the energy level E_1 , see Fig. 15. By taking the energy of the elastic spring into account, we can then write the transition rates in the form

$$\begin{aligned} k_+(y, \beta) &= k \exp[-\beta [E_0 + \max\{y + 1/2, 0\}]], \\ k_-(y, \beta) &= k \exp[-\beta [E_1 + \max\{-y - 1/2, 0\}]]. \end{aligned}$$

where $E_1 = E_0 + v_0$ and the common pre-factor k defines the characteristic time scale for a single well system. If $y > -1/2$, then only the energy barrier from the unfolded to the folded state depends on y , see Fig. 15(a). In this case, the rates can be written in the form

$$k_+(y, \beta) = k_- \exp[-\beta (y - y_0)] \quad (22a)$$

$$k_-(y, \beta) = k \exp[-\beta E_1] = \text{const} \quad (22b)$$

and the timescale of the jump process is $\tau = 1/k_- = k^{-1} \exp[\beta E_1]$. If $y < -1/2$, see Fig. 15(b), then we obtain instead

$$k_+(y, \beta) = k_- \exp[\beta v_0] = \text{const}.$$

$$k_-(y, \beta) = k_- \exp[\beta (y - y_0 + v_0)].$$

We see in Fig. 15 that, in response to shortening, the overall transformation rate $\tilde{k} = k_+ + k_-$ first increases exponentially as the forward barrier is lowered (while the reverse barrier remains constant) and then decreases as the reverse barrier is elevated (while the forward barrier remains constant). In addition, we see that for large stretching $\tilde{k} \approx k_-$ and for large shortening $\tilde{k} \approx k_- \exp[\beta v_0]$.

Note that HS considered only the case $y > -1/2$, see Fig. 15(a). To see why the value $y = -1/2$ is special in the muscle context, we recall that in this case the unloaded system is symmetric, $\langle p \rangle = 1/2$. Then the tension during the purely elastic phase of the fast force recovery (when $\langle p \rangle$ remains constant) is $\sigma = y + 1/2$, which becomes negative exactly at $y = -1/2$. In experiments on muscles, the relaxation rates have been measured only for $y > -1/2$ because below this threshold muscle fibers are usually subjected to buckling. Our analysis suggests that near the regimes with $y = -1/2$ the step size dependence of the rate of fast force recovery may deviate from exponential.

The results of numerical simulations of stochastic hopping for a single HS element subjected to a quasistatic stretching are shown in Fig. 16. For $y < y_0$ the spin variable spends most of the time in the folded conformation ($x = -1$). When the loading device approaches the point $y = y_0$, the flips between the wells become more frequent before finally the system stabilizes again in the unfolded configuration ($x = 0$).

The stochastic dynamics shown in Fig. 16 can also be seen through the prism of the deterministic evolution of a single-particle probability distribution $\rho_1(t)$. For a generic test function q we can write

$$\begin{aligned} d\langle q(x) \rangle &= q(-1) [\rho_1(-1, t + dt) - \rho_1(-1, t)] \\ &\quad + q(0) [\rho_1(0, t + dt) - \rho_1(0, t)], \end{aligned}$$

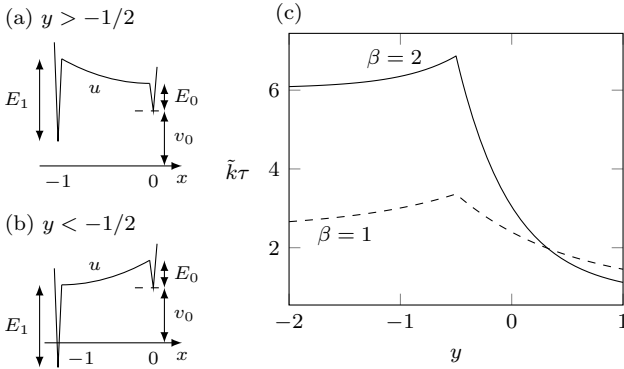


FIG. 15. Schematic representation of the energy barrier in the HS bistable potential. The energy barriers corresponding to the transition rates in the absence of elastic contribution are denoted E_1 and E_2 . We define the characteristic timescale by $\tau = \exp[\beta E_1]$. (a) Energy landscape for $y > -1/2$ which is the case considered in Ref. [1]; (b) energy landscape for $y < -1/2$ not considered by HS. (c), Relaxation rate as function of the total elongation y for $\beta = 1$ (dashed line) and $\beta = 2$ (solid line).

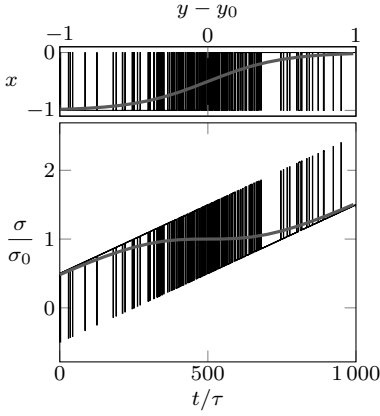


FIG. 16. Hopping response to a ramp stretch from $y = y_0 - 1$ to $y = y_0 + 1$ (single trajectory with jumps hardly distinguishable around $y = y_0$). The time step is $\Delta t = 10^{-3}\tau$ and the time is measured in the units of τ . The average trajectory is shown by the gray line. Here $\beta = 4$.

then, using (21), we obtain

$$d\langle q(x) \rangle = q(-1) \{k_+[1 - \rho_1(-1, t)] - k_- \rho_1(-1, t)\} dt + q(0) \{k_-[1 - \rho_1(0, t)] - k_+ \rho_1(0, t)\} dt.$$

In the limit $dt \rightarrow 0$, we obtain exactly the HS kinetic equation

$$\frac{\partial}{\partial t} \rho_1(t) = k_+(y) [1 - \rho_1(t)] - k_-(y) \rho_1(t). \quad (23)$$

Its general solution can be written as

$$\rho_1(t) = \rho_1(0) \exp[-A(t)] + \int_0^t \tilde{k}(t') \exp[A(t') - A(t)] \rho_1^\infty(y(t)) dt',$$

where $A(t) = \int_0^t \tilde{k}(t') dt'$ and $\rho_1^\infty = k_+/\tilde{k}$ is the stationary distribution (2). Since $\langle x \rangle = \rho_1$, this equation describes the time dependence of the average configuration shown in Fig. 16 by the gray line.

The comparison of individual stochastic trajectories with the evolution of averages shows that the information about individual flips, potentially measurable in single molecule experiments, gets lost in the chemomechanical description. In particular, near the point $y = y_0$, fluctuations play a dominant role in the stochastic description, as is suggested by our equilibrium theory, while from the chemomechanical perspective this particular state is completely indistinguishable from the other equilibrium states.

B. Bundle of HS elements

The isothermal discrete dynamics of a system with N elements can be described in terms of the macroscopic parameter $p \in \{0, 1/N, \dots, 1\}$. If only one transition occurs

between the time t and the time $t + dt$, then the function $p(t)$ is a one dimensional random walk (see Fig. 14), governed by the jump probabilities

$$\begin{aligned} \mathbb{P}[p^{t+dt} = p^t + 1/N] &= \phi_+(p^t; y, \beta) dt & (24a) \\ \mathbb{P}[p^{t+dt} = p^t - 1/N] &= \phi_-(p^t; y, \beta) dt. & (24b) \end{aligned}$$

where $\phi_+(p; y, \beta) = N(1-p)k_+(y, \beta)$ and $\phi_-(p; y, \beta) = Np k_-(y, \beta)$. Following a similar procedure as the one leading to Eq. (23), we obtain the master equation for the probability distribution $\rho(p, t)$

$$\begin{aligned} \frac{\partial}{\partial t} \rho(p, t; y, \beta) &= \phi_+(1-p+1/N; y) \rho(p-1/N, t; y, \beta) \\ &+ \phi_-(p+1/N; y) \rho(p+1/N, t; y, \beta) \\ &- [\phi_+(1-p; y) + \phi_-(p; y)] \rho(p, t; y, \beta), \end{aligned} \quad (25)$$

which can be solved numerically since we know the tridiagonal transfer matrix of the process at each time step. It is clear, however, that since the transition probabilities (21) depend only on the control parameter y , the trajectories of individual elements are independent. Hence, at a given y each macro-configuration can be viewed as a realization of N Bernoulli processes with the probability of success $\rho_1(t)$ solving Eq. (23). Therefore the probability density $\rho(p, t) = \mathbb{P}(p^t = p)$ is a binomial distribution with parameters N and $\rho_1(t)$:

$$\rho(p, t) = \binom{N}{Np} [\rho_1(t)]^{Np} [1 - \rho_1(t)]^{N-Np}. \quad (26)$$

One can verify that that (26) solves (25) and since $\langle p \rangle(t) = \rho_1(t)$, Eq. (23) can be viewed as the analog of Eq. (9) in Ref. [1]. We have then shown that the dynamics of the entire distribution is enslaved to the dynamics of the order parameter $\langle p \rangle(t)$ captured by the original HS model. It is also clear that in the long time limit the distribution (26) converges to the Boltzmann distribution (10).

h. Quasistatic loading. To illustrate the fact that our dynamical model is fully compatible with the equilibrium behavior studied in Sec. IIB, we now consider the quasistatic driving of a cluster of N HS elements, see Fig. 17. The behavior of the individual trajectories generated by the stochastic random walk Eq. (24) is shown for $N = 10$ (light gray) and $N = 100$ (dark gray). The system is subjected to continuous stretching from $y = y_0 - 1$ to $y = y_0 + 1$ over the time interval $[0, 10^3 \tau]$ with the temperature remaining constant; this loading protocol mimics the unzipping tests for biological macromolecules [12, 15, 18, 55]. The results were obtained using the same numerical procedures as in the case of a single element.

The stochastic evolution of the order parameter p and of the corresponding tension are illustrated in Fig. 17. Together with single trajectories, we show the evolution of the average (solid black line) obtained from Eq. (23) and the corresponding equilibrium response curves (open

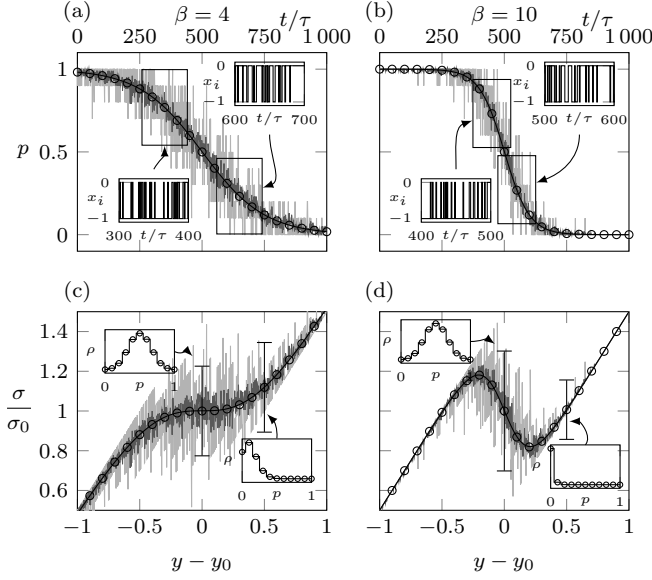


FIG. 17. Response of the HS model to a ramp loading from $y_0 - 1$ to $y_0 + 1$ achieved in 1000τ , for $\beta = 4$ [(a) and (c)] and $\beta = 10$ [(b) and (d)]. Individual stochastic trajectories are shown for $N = 10$ (light gray) and $N = 100$ (dark gray). [(a) and (b)] Evolution of the order parameter p . The inserts show two samples of a single trajectory around the point where $p = 1/2$. [(c) and (d)] Tension-elongation relations obtained from $\sigma = y + p$. The inserts show the marginal distribution ρ at the two different times indicated by the vertical bars. Solid lines represent the thermal equilibrium averages given by Eq. (14) and Eq. (7) and open symbols show the solutions of the HS kinetic equation (23) and the distribution (26).

circles). The inserts in Figs. 17(a) and 17(b) show samples of the trajectories for single elements computed from (21).

Observe that individual trajectories reveal at finite N a succession of jumps describing individual folding-unfolding events as is suggested by the analysis of the marginally equilibrated system. As the number of element increases the fluctuations of p decrease in accordance with our Eq. (16), and a single realization trajectory (dark gray) gets close to the average trajectory (black).

In the inserts in Figs. 17(c) and 17(d) we show the probability density ρ obtained from (26) at different times (solid line) together with the equilibrium density (open circles). As expected, the distribution does not depend on temperature at $y = y_0$ while becoming progressively more localized away from this point.

To make the stochastic fluctuations more visible, we compare in Fig. 18 the variance of the order parameter p obtained from the stochastic model (24) (gray lines) with the results of the analytic computations based on the kinetic equation (26) (thin lines) and the equilibrium model, see Eq. (16) (open circles). The system contains $N = 10$ elements and each stochastic trajectory corresponds to 10^4 realizations of our random walk. We see

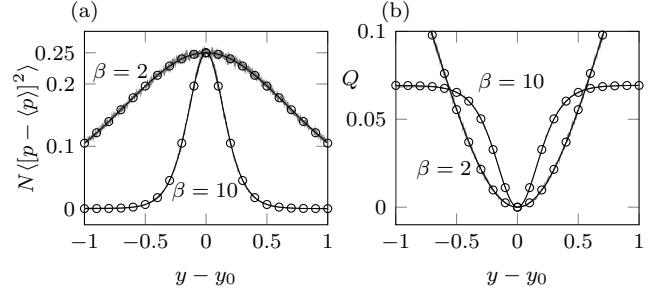


FIG. 18. Evolution of the normalized variance $N\langle(p - \langle p \rangle)^2\rangle$ and the heat release as function of the elongation during a quasistatic stretching between $t = 0$ and $t = 10^3\tau$. For each temperature we show the analytic computations from (16) and (9) (open circles), the results of the stochastic model (24) corresponding to 10^4 independent realizations with $N = 10$ (gray lines) and the solution based on the solution of the kinetic equations (23) and (26) (thin lines).

that stochastic simulations are fully compatible with the predictions of equilibrium theory, in particular, we see once again that the normalized variance reaches a maximum at $y = y_0$ becoming independent of the temperature.

i. Fast loading. In addition to averages, captured already by the chemomechanical kinetic equation (23), the master equation (25) allows one to follow the evolution of higher order moments. To illustrate this point, we now show how the HS system responds to abrupt perturbations which is exactly the type of mechanical test conducted in Ref. [1], see Fig. 19. The system is first maintained in equilibrium at $y = y_0 = 0.5$ before an instantaneous length change (to $y = 0$.) is applied. This protocol is repeated for systems with $N = 10$ (dotted lines) and $N = 100$ (solid line). Again, individual real-

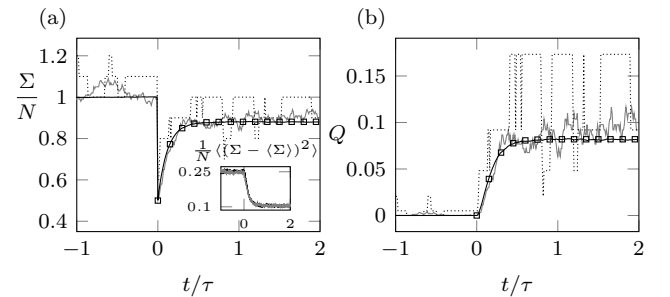


FIG. 19. Stochastic simulation of a quick force recovery in response to a step of $y - y_0 = -0.5$. (a) Tension per cross-linker; (b) heat released. Dotted lines: Single stochastic trajectory for a system with $N = 10$; gray line single trajectory with $N = 100$; solid line average over 1000 trajectories with $N = 10$; squares, response obtained using the HS kinetic equation (23). Inserts in (a), gray (respectively, solid) line, fluctuations obtained using 1000 realizations for $N = 100$ (respectively, $N = 10$). Here $\beta = 4$ and $y_0 = 0.5$.

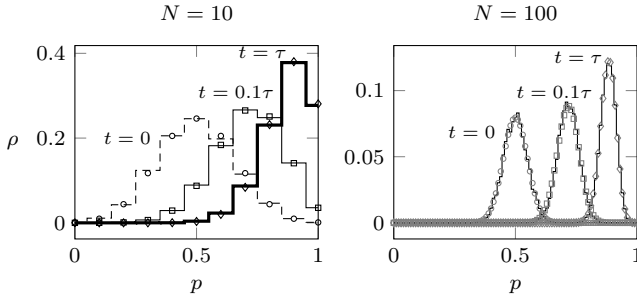


FIG. 20. Time evolution (snapshots) of the probability density $\rho(p, t; y, \beta)$ showing gradual equilibration of the system subjected to an abrupt shortening. Lines: histograms obtained from 10^4 trajectories; symbols distributions recovered from the first order kinetic equations (23) and (26). Parameters are the same as described in the caption to Fig. 19

izations may strongly depart, especially at low N , from the average behavior described by the HS reaction equation (23) (symbols).

These fluctuations can also be seen from the dynamics of the density ρ which is reconstructed from a large number of sample trajectories/experiments in Fig. 20. We observe that for a system with a small number of elements [see Fig. 20(a), $N = 10$] the probability distribution remains broad even after the recovery while, for a system with large N [see Fig. 20(b), $N = 10$], the distribution is sharply peaked throughout the process. Again, we find a perfect agreement between the distribution obtained from the Monte-Carlo simulations (lines) and the one recovered from the knowledge of the averaged behavior given by the HS kinetic equation parametrizing the binomial distribution (26) (symbols).

IV. SKELETAL MUSCLES

The development of the HS model was originally motivated by the mechanical experiments involving rapid shortening of skeletal muscles with the goal of distinguishing passive from active contributions to tension recovery [1, 56–59]. It was shown that the first phase of the response to a quasi-instantaneous shortening imposed on a maximally activated (tetanized) single muscle fiber represents a purely elastic force drop. During the second phase, the tension recovers to a level which depends nonlinearly on the amplitude of the shortening. This fast force recovery, lasting about 1 ms, precedes a considerably slower phase at the end of which the tension fully returns to its original value. The latter, taking place on a 100-ms time scale, is usually interpreted as an *active* process driven by ATP hydrolysis [7, 60].

j. Biochemistry vs mechanics. In their classical 1971 paper HS conjectured that the force recovery at the *ms* time scale must be attributed to a rapid folding in an assembly of attached cross-bridges linking actin and myosin filaments. The idea of bistability in the structure

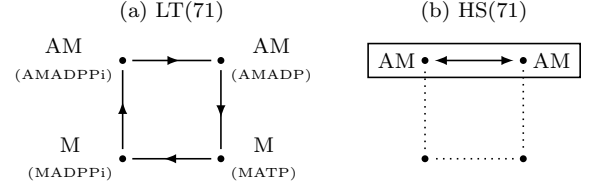


FIG. 21. Biochemical vs purely mechanistic description of the power stroke in skeletal muscles: (a) The Lymn-Taylor four-state cycle, LT(71) and (b) the Huxley-Simmons two-state cycle, HS (71).

of myosin heads, giving rise to the concept of a power stroke, has been later fully supported by crystallographic studies [61, 62].

While the scenario proposed by HS is in agreement with the fact that the power stroke is the fastest step in the Lymn-Taylor (LT) enzymatic cycle [63, 64], there is a subtle formal disagreement with the existing biochemical picture, see Fig. 21. Thus, HS assumed that the mechanism of the fast force recovery is fully *passive* and can be reduced to a mechanically induced conformational change. In contrast, the LT cycle for actomyosin complexes is based on the assumption that the power stroke can be reversed only *actively* through the completion of the biochemical pathway including ADP (adenosine diphosphate) release, myosin unbinding, binding of uncleaved ATP (adenosine triphosphate), splitting of ATP into ADP and P_i , and then rebinding of myosin to actin [6, 63].

In other words, while HS postulated that thermal fluctuations experienced by the attached myosin heads can be biased by external loading and that the power stroke can be reversed by mechanical means, most of the biochemical literature is based on the assumption that the power-stroke recocking cannot be accomplished without the presence of ATP. In particular, physiological fluctuations in muscle response are mostly addressed in the context of *active* behavior [65–71].

Some authors, however, follow the HS mechanistic approach in assuming that the power-stroke-related leg of the LT cycle can be decoupled from the rest of the biochemical pathway; see, for instance, Refs [49, 72]. Below we adopt this perspective, which implies that at a 1-ms time scale the mechanism dominating muscle response is a purely mechanical folding-unfolding. We then collect specific predictions, generated by our augmented HS model, and use them as a guidance in designing new experiments aimed, in particular, at verifying the correctness of the underlying purely mechanistic model.

k. Thermal effects. The knowledge of the free energy of the HS system allows one to assess not only mechanical but also thermal manifestations of the fast force recovery. The latter have been measured in experiments employing calorimetric techniques [49, 50, 73], however, a thermomechanical interpretation of these experiments in the HS framework is still an open question.

For instance, studies of the heat exchange following the application of a fast length drop showed an increase of temperature at the time scale of the purely elastic response followed by a slower cooling during the force recovery up to a level which is higher than the baseline preceding the step. While, the temperature decay was linked to the equilibrium heat effect of the conformational change, which was assumed to be negative [73], the HS model predicts a positive heat effect because a “mixed” state with high entropy is transformed into a “pure” state with low entropy.

More specifically, the HS-type interpretation of the temperature measurements during the fast force recovery would be as follows:

(i) The rapid increase of temperature recorded during the applied length step is a reflection of an adiabatic temperature increase. To justify this claim, we mention that several experimental studies of muscles, involving temperature changes due to rapid switching between, solutions showed that the time scale of temperature equilibration within a typical muscle fiber is of the order of 10 ms [74, 75], which is 10 times slower than the duration of the fast force recovery process.

(ii) The subsequent temperature decay is an outcome of the cooling due to heat conduction and the heat release due to the conformational change. The fact that the temperature at the end of the recovery is higher than the baseline temperature is a signature of the exothermic nature of the folding process (of the working-stroke) and the inefficiency of the heat removal mechanism at this time scale.

Several groups have also addressed the influence of temperature on the force generation either by performing mechanical experiments in different solutions [45, 46] or by applying rapid temperature changes to tetanized muscle fibers [47, 48, 76]. In both cases the experiments show that the isometric tension increases with temperature while the conformational state of the cross-bridges becomes more homogeneous. Such a response in the case of fast adiabatic changes can be explained by the fact that, in order to maintain the value of the entropy at higher temperature, the HS system must evolve towards a more ordered configuration. This effect, however, is not captured by the HS model where temperature does not affect the value of isometric tension at $y = y_0$, see our Fig. 3. To describe quantitatively the temperature dependence of the tension-elongation curves, we may augment the HS model by assuming phenomenologically that the energy bias v_0 is a function of temperature [46].

While the value of the isometric tension may depend significantly on temperature, experiments show that the slope of the tension-elongation curve is only weakly temperature sensitive [49]. In general, the HS model predicts considerable dependence of the shape of the tension-elongation relation on temperature, including the possibility of negative stiffness which is not observed in experiment. However, in the range of temperatures considered in experiment (no more than 20°C) this effect is weak.

For instance, if we assume that the mechanical properties of the cross-bridges are not affected by temperature, as is observed in experiments [45], and take $\beta = 4$ at $T = 4^\circ\text{C}$, we obtain $\beta \sim 3.8$ at $T = 24^\circ\text{C}$. In the HS model, the sensitivity of the equilibrium tension-elongation curves to such variations of β is negligible.

Among other interesting thermomechanical effects, invoked by the HS model, we mention the “infinite” cooling in the process of reaching the state of isometric contractions. To observe this effect the muscle must be first equilibrated after shortening (at the T_2 state) and then stretched back to the T_0 state.

l. Fluctuations. While in myofibrils half-sarcomeres fluctuations can be expected to average out, at the scale of an elementary acto-myosin complex (our half-sarcomere, see Fig. 11), where $N \sim 10^2$, fluctuations may interfere with experiments. For instance, as we have seen in our Fig. 17 and Fig. 19, the abrupt transitions associated with conformational changes in individual cross-bridges may produce measurable steps in the response curves.

Another way of assessing the role of fluctuations is through the measurement of equilibrium susceptibilities. Thus, the effective stiffness of the HS bundle can be represented as a sum of an enthalpic term describing zero-temperature elasticity and an entropic term that can be evaluated from the measurements of tension fluctuations. More specifically, given that such fluctuations can be measured, our Eq. (20) allows one to track the number of the attached elements at different degrees of stretching and different temperatures.

On the other hand, in mechanical experiments conducted on single fibers and involving x-ray diffraction measurements [77], one can, in principle, test the prediction of the model that the configuration with $\langle p \rangle = 1/2$ is the state of maximum disorder. By studying statistics of the observed fluctuations in the steady states, one can also search for deviations from the static fluctuation-dissipation relation (5). If found, then they may reveal the presence of out-of-equilibrium active processes at the time scales of fast force recovery which would then reconcile the mechanical and the biochemical pictures of this phenomenon [78].

m. Cooperativity. Statistics of fluctuations for groups of myosins has been studied exhaustively in experiments involving *active* contraction. Considerable coordination between individual elements was detected, responsible for synchronized oscillations in close to stall conditions (our point $y = y_0$) [56, 79–84]. The cooperative behavior was explained by the fact that, due to the presence of long-range elastic interactions transmitted through compliant backbones, the mechanical state of one motor influences the kinetics of other motors [40, 41]. The implied myosin-myosin coupling was taken into consideration in models addressing active behavior of motor groups [85, 86] and emergent phenomena characterized by large-scale entrainment signatures were identified [29, 65, 66, 87, 88]. The claims that activity in

such systems is crucial for the emergence of synchronized oscillations were supported by *in vitro* assays [65, 66] showing that the finite size scaling of the fluctuations is fundamentally differs from the equilibrium one $N^{-1/2}$.

It is clear that to capture this effect, the original HS model with rigid backbone and controlled displacement has to be generalized, but the actual role of activity in synchronization of cross-bridges is not obvious. Thus, it has been recently argued [2] that the dominant factor behind collective behavior is not activity but the long-range interactions between cross-bridges. The simplest way to create such “cross-talk” without leaving the HS framework is to consider the response of a HS system subjected to a constant force (soft device) rather than a constant displacement [26]. It has been shown that in the systems of this type the nonconvexity of the free energy can resist thermal fluctuations at sufficiently low temperatures, giving rise to macroscopic cooperativity. Moreover, in the case of soft and mixed (soft-hard) loadings, the pseudocritical point of HS at $\beta = 4$ becomes a real critical point of the Curie type around which fluctuations diverge in the thermodynamic limit and can show unusual finite-size scaling [2].

V. NONMUSCLE SYSTEMS

The prototypical nature of the HS model makes it relevant outside the skeletal muscle context as well. In fact, it can be viewed as a description of a large class of biological systems involving collectively biased multistable elements and exhibiting, as a result, sigmoidal or ultrasensitive response at finite temperatures as in our Fig. 2(a). The HS model describes, perhaps, the most elementary molecular system capable of transforming in a Brownian environment a continuous input into a binary, all-or-none output that is crucial for the fast and efficient, stroke-type behavior.

We recall that the capacity of multisite systems to flip in a reversible fashion between several metastable conformations is essential for many processes in cellular physiology, including cell signaling, cell movement, chemotaxis, differentiation, and selective expression of genes [89, 90]. Usually, both the input and the output in such systems, known as allosteric, are assumed to be of biochemical origin. The HS model, dealing with *mechanical* response and relying on *mechanical* driving, complements biochemical models and presents a different perspective on allostery.

n. Hair cell gating. Our first example of hypersensitivity concerns the transduction channels in hair cells [91]. Each hair cell contains a bundle of $N \approx 50$ stereocilia which are mechanically stimulated by the vibrations in the inner ear. The stereocilia possess transduction channels closed by “gating springs” which can open (close) in response to a positive (negative) shear strain X , imposed on the cilia from outside.

The broadly accepted model of this phenomenon [10]

views the hair bundle as a set of N bistable springs arranged in parallel. It is identical to the HS model if the folded (unfolded) configurations of cross-bridges are identified with the closed (opened) states of the channels. The applied loading, which tilts the potential and biases in this way the distribution of closed and open configurations, is treated in this model as a hard device of HS.

To stress the equivalence of the results, it is enough to mention the expression for the total stiffness of a hair bundle obtained in Ref. [10], which is a direct analog of our Eq. (15). Moreover, the mechanical experiments, involving a mechanical solicitation of the hair bundle through an effectively rigid glass fiber showed that the stiffness of the hair bundle is negative around the physiological functioning point of the system [11], which is fully compatible with the predictions of the HS model.

o. Cell adhesion. A similar analogy can be drawn between the HS model and the models of collective unzipping for adhesive clusters [9, 92–95]. At the micro-scale we again deal with N elements representing, for instance, integrins or cadherins, that are attached in parallel to a common, relatively rigid pad. The two conformational states, which can be described by a single spin variable, are the bound and the unbound configurations.

The binding-unbinding phenomena in a mechanically biased system of the HS type are usually described by the Bell model [8], which is a soft device analog of the HS model with $\kappa_0 = \infty$. In this model the breaking of an adhesive bond represents an escape from a metastable state and the corresponding rates are computed by using Kramers’ theory [95, 96] as in the HS model. In particular, the rebinding rate is often assumed to be constant [97, 98], which is also the assumption of HS for the reverse transition from the post- to the pre-power-stroke state. More recently, Bell’s model was generalized through the inclusion of ligand tethers, bringing a finite value to κ_0 and using the master equation for the probability distribution of attached units [9, 97].

The main difference between the Bell-type models and the HS model is that the detached state cannot bear force while the unfolded conformation can. As a result, while the cooperative folding-unfolding (ferromagnetic) behavior in the HS model is possible in the soft device setting [2], similar cooperative binding-unbinding in the Bell model is impossible because the rebinding of a fully detached state has zero probability. To obtain cooperativity in models of adhesive clusters, one must use a mixed device, mimicking the elastic backbone and interpolating between soft and hard driving [9, 26, 95, 99].

p. Synaptic fusion. While muscle tissues maintain stable architecture over long periods of time, it is feasible that transitory muscle-type structures can be also assembled to perform particular functions. An interesting example of such assembly is provided by the SNARE proteins responsible for the fast release of neurotransmitters from neurons to synaptic clefts. The fusion of synaptic vesicles with the presynaptic plasma membrane [22, 100] is achieved by mechanical zipping of the SNARE com-

plexes which can in this way transform from opened to closed conformation [101].

To complete the analogy, we mention that individual SNAREs participating in the collective zipping are attached to an elastic membrane that can be mimicked by an elastic or even rigid backbone [102]. The presence of a backbone mediating long-range interactions allows the SNAREs to cooperate in fast and efficient closing of the gap between the vesicle and the membrane. The analogy with muscles is corroborated by the fact that synaptic fusion takes place at the same time scale as the fast force recovery (1 ms) [103].

q. Macromolecular hairpins. Another class of phenomena that can be rationalized within the HS framework is the ubiquitous flip-flopping of macro-molecular hairpins subjected to mechanical loading [12–14, 16].

We recall that in a typical experiment of this type, a folded (zipped) macromolecule is attached through compliant links to micron-sized beads trapped in optical tweezers. As the distance between the laser beams is increased, the force applied to the molecule rises up to a point where the subdomains start to unfold. An individual unfolding event may correspond to the collective rupture of N molecular bonds or an unzipping of a hairpin. The corresponding drops in the force accompanied by an abrupt increase in the total stretch can lead to an overall negative stiffness response [12, 15, 55].

Realistic examples of unfolding in macromolecules may involve complex “fracture” avalanches [19] that cannot be modeled by using the original HS model. However, the HS theoretical framework is general enough to accommodate hierarchical meta-structures whose stability can be also biased by mechanical loading. In fact, the importance of the topology of interconnections among the bonds and the link between the collective nature of the unfolding and the dominance of the HS-type parallel bonding have been long stressed in the studies of protein folding [104]. The broad applicability of the HS mechanical perspective on collective conformational changes is also corroborated by the fact that proteins and nucleic acids exhibit negative stiffness and behave differently in soft and hard devices [18, 20, 21].

The ensemble dependence in these systems suggests that additional structural information can be obtained if the unfolding experiments are performed in the mixed device setting. The type of loading may be affected through the variable rigidity of the “handles” [105, 106] or the use of an appropriate feedback control that can be modeled in the HS framework by a variable backbone elasticity.

r. Allosteric systems. As we have already mentioned, collective conformational changes in distributed biological systems containing coupled bistable units can be driven not only mechanically, by applying forces or displacements, but also biochemically by, say, varying concentrations or chemical potentials of ligand molecules in the environment [107]. Such systems can become ultrasensitive to external stimulations as a result of the interaction between individual units undergoing conforma-

tional transformation which gives rise to the phenomenon of allostery also known as conformational spread [90, 108]. The switch-like input-output relations are required in a variety of biological applications because they ensure both robustness in the presence of external perturbations and ability to quickly adjust the configuration in response to selected stimuli [89, 109]. The mastery of control of biological machinery through mechanically induced conformational spread is an important step in designing efficient biomimetic nanomachines [35, 110–112].

To link this behavior to the HS model, we note that the amplified *dose response*, characteristic of allostery, is analogous to the sigmoidal *stress response* of the paramagnetic HS system where an applied displacement plays the role of the controlled input of a ligand. Usually, in allosteric protein systems, the ultrasensitive behavior is achieved as a result of nonlocal interactions favoring all-or-none types of responses; moreover, the required long-range coupling is provided by mechanical forces acting inside membranes and molecular complexes. In the HS model such coupling is modeled by the parallel arrangement of elements, which preserves the general idea of non-locality. Despite its simplicity, the appropriately generalized HS model [2] captures the main patterns of behavior exhibited by allosteric systems, including the possibility of a critical point mentioned in Ref. [107].

VI. CONCLUSIONS

In this paper we presented a perspective on the seminal work of Huxley and Simmons by viewing their results through the prism of statistical mechanics. This allowed us to place an emphasis on thermal effects and equilibrium fluctuations that cannot be ignored in many biological applications of the HS model.

The chemomechanical approach of HS is based on the description of a mechanical system with N elements in a thermal bath in terms of a single deterministic reaction equation. Instead, our analysis starts with the analogy between the HS model in a hard device and the paramagnetic Ising model where the average conformation of a cross-bridge viewed as the counterpart of magnetization. In view of this analogy, the HS model describes a size indifferent mean-field statistical mechanical system which explains why the many-body stochastic dynamics can be modeled by a single chemical reaction. The analogy with paramagnetism is, however, not complete, as is revealed by the phenomena of negative susceptibility and pseudo-criticality that we identify with the HS model. In particular, we show that while genuine criticality requires cooperativity, in the HS model the collective response is imposed through the rigid backbone rather than being an emergent property.

Some of the most interesting findings of this paper concern the thermal properties of the HS system. Thus, our analysis highlights the previously unnoticed temperature robustness of the pseudocritical state where specific

heat vanishes and fluctuations become temperature independent. We also quantified the temperature variations during fast unfolding and demonstrated that isothermal and adiabatic responses may differ. These observations point towards the importance of the nonorthodox experimental protocols combining mechanical and calorimetric measurements. In particular, the revealed fluctuation dependence of equilibrium susceptibilities suggests a non-crystallographic way for the evaluation of the number of folding elements.

To account for fluctuations in kinetics we, following Refs. [29, 30], went beyond the reaction-based modeling of the averages and studied the time dependence of the probability distributions for various parameters during mechanical transients. The results of the deterministic model of HS are, of course, recovered from the analysis of the evolution of the first moments of these distributions.

While being the simplest mean-field description of a broad class of biological phenomena, the HS model clearly misrepresents the important elastic coupling between the folding elements, as has been long realized in muscle physiology [40, 41]. This drawback can be remedied by taking into account the mechanical feedback induced by the backbone elasticity [2] resulting in various

degrees of synchronization already at zero temperature [26]. A more important limitation of the HS model is the neglect of the ATP-fueled activity which can crucially interfere with passive folding [29, 65, 66, 85–88, 113]. The account of nonthermal driving in the HS setting produces new qualitative effects [78, 114] which opens the possibility to build a fully mechanistic analog of the enzymatic cycle originating in the work of Lymn and Taylor. Quantitative applications of the HS model in and outside the muscle context also call upon the account of complex geometry, hierarchical architecture, soft-spin-type multistability, and short-range interactions. All these potential augmentations, however, will not diminish the role of the original HS model as a source of fundamental physical intuition about the behavior of a wide class of biological systems.

VII. ACKNOWLEDGMENTS

The authors thank R. Sheshka, P. Recho, T. Lelièvre and J.-M. Allain and the anonymous reviewers for helpful comments.

-
- [1] A. F. Huxley and R. M. Simmons, *Nature* **233**, 533 (1971).
 - [2] M. Caruel, J. M. Allain, and L. Truskinovsky, *Phys. Rev. Lett.* **110**, 248103 (2013).
 - [3] T. L. Hill, *Prog. Biophys. Molec. Biol.* **29**, 105 (1976).
 - [4] A. F. Huxley and S. Tideswell, *J. Muscle Res. Cell M.* **17**, 507 (1996).
 - [5] G. Piazzesi and V. Lombardi, *Biophys. J.* **68**, 1966 (1995).
 - [6] D. Smith, M. Geeves, J. Sleep, and S. Mijailovich, *Ann. Biomed. Eng.* **36**, 1624 (2008).
 - [7] M. Linari, M. Caremani, and V. Lombardi, *P Roy. Soc. Lond. B Bio.* **277**, 19 (2010).
 - [8] G. Bell, *Science* **200** (1978).
 - [9] T. Erdmann and U. S. Schwarz, *Eur. Phys. J. E* **22**, 123 (2007).
 - [10] J. Howard and A. J. Hudspeth, *Neuron* **1**, 189 (1988).
 - [11] P. Martin, A. Mehta, and A. Hudspeth, *Proc. Natl. Acad. Sci. U.S.A.* **97**, 12026 (2000).
 - [12] J. Liphardt, B. Onoa, S. B. Smith, I. Tinoco, and C. Bustamante, *Science* **292**, 733 (2001).
 - [13] N. Bosaeus, A. H. El-Sagheer, T. Brown, S. B. Smith, B. Åkerman, C. Bustamante, and B. Norden, *Proc. Natl. Acad. Sci. U.S.A.* **109**, 15179 (2012).
 - [14] M. T. Woodside, C. Garcia-Garcia, and S. M. Block, *Curr. Opin. Chem. Biol.* **12**, 640 (2008).
 - [15] A. N. Gupta, A. Vincent, K. Neupane, H. Yu, F. Wang, and M. T. Woodside, *Nat Phys* **7**, 631 (2011).
 - [16] A. Prados, A. Carpio, and L. L. Bonilla, *Phys. Rev. E* **86**, 021919 (2012).
 - [17] V. Muñoz, E. R. Henry, J. Hofrichter, and W. A. Eaton, *Proc. Natl. Acad. Sci. U.S.A.* **95**, 5872 (1998).
 - [18] T. Bornschlöggl and M. Rief, *Phys. Rev. Lett.* **96**, 118102 (2006).
 - [19] A. Srivastava and R. Granek, *Phys. Rev. Lett.* **110**, 138101 (2013).
 - [20] U. Gerland, R. Bundschuh, and T. Hwa, *Biophysj* **84**, 2831 (2003).
 - [21] N. Thomas and Y. Imafuku, *J Theor Biol* **312**, 96 (2012).
 - [22] T. C. Südhof, *Neuron* **80**, 675 (2013).
 - [23] L. L. Bonilla, A. Carpio, A. Prados, and R. R. Rosales, *Phys. Rev. E* **85**, 031125 (2012).
 - [24] T. L. Hill, *Prog. Biophys. Molec. Biol.* **28**, 267 (1974).
 - [25] L. Marcucci and L. Truskinovsky, *Phys. Rev. E* **81** (2010).
 - [26] M. Caruel, J.-M. Allain, and L. Truskinovsky, *J. Mech. Phys. Solids* **76**, 237 (2015).
 - [27] S. Pradhan, A. Hansen, and B. K. Chakrabarti, *Rev. Mod. Phys.* **82**, 499 (2010).
 - [28] R. Balian, *From Microphysics to Macrophysics*, Methods and Applications of Statistical Physics (Springer Science & Business Media, 2006).
 - [29] A. Vilfan and T. Duke, *Biophys. J.* **85**, 818 (2003).
 - [30] T. Erdmann, P. J. Albert, and U. S. Schwarz, *J. Chem. Phys.* **139**, 175104 (2013).
 - [31] J. S. Rowlinson, *Liquids and liquid mixtures*, Modern aspects series of chemistry (Butterworths, London, 1959).
 - [32] D. R. Squire, A. C. Holt, and W. G. Hoover, *Physica* **42**, 388 (1969).
 - [33] J. F. Lutsko, *J. Appl. Physiol.* **65**, 2991 (1989).
 - [34] J. P. Wittmer, H. Xu, P. Políńska, F. Weysser, and J. Baschnagel, *J. Chem. Phys.* **138**, 191101 (2013).
 - [35] Z. Wu, R. Harne, and K. Wang, *J. Intell. Mat. Syst. Struct.* **27**, 1189 (2016).

- [36] E. Eisenberg and T. Hill, *Prog. Biophys. Molec. Biol.* **33**, 55 (1978).
- [37] L. E. Ford, A. F. Huxley, and R. M. Simmons, *J. Physiol.* **269**, 441 (1977).
- [38] L. E. Ford, A. F. Huxley, and R. M. Simmons, *The Journal of physiology* **311**, 219 (1981).
- [39] H. Kojima, A. Ishiura, and T. Yanagida, *Proc. Natl. Acad. Sci. U.S.A.* **91**, 12962 (1994).
- [40] K. Wakabayashi, Y. Sugimoto, H. Tanake, Y. Ueno, Y. Takezawa, and Y. Amemiya, *Biophys. J.* **67**, 2422 (1994).
- [41] H. Huxley, A. Stewart, H. Sosa, and T. Irving, *Biophys. J.* **67**, 2411 (1994).
- [42] G. Piazzesi, M. Reconditi, M. Linari, L. Lucii, P. Bianco, E. Brunello, V. Decostre, A. Stewart, D. B. Gore, T. C. Irving, M. Irving, and V. Lombardi, *Cell* **131**, 784 (2007).
- [43] M. Irving, G. Piazzesi, L. Lucii, Y. Sun, J. Harford, I. Dobbie, M. Ferenczi, M. Reconditi, and V. Lombardi, *Nat. Struct. Biol.* **7**, 482 (2000).
- [44] A. V. Hill, *P Roy. Soc. Lond. B Bio.* **126**, 136 (1938).
- [45] G. Piazzesi, A. Reconditi, N. Koubassova, V. Decostre, M. Linari, L. Lucii, and V. Lombardi, *J. Physiol.* **549**, 93 (2003).
- [46] V. Decostre, P. Bianco, V. Lombardi, and G. Piazzesi, *Proc. Natl. Acad. Sci. USA* **102**, 13927 (2005).
- [47] K. W. Ranatunga, M. E. Coupland, G. J. Pinniger, H. Roots, and G. W. Offer, *J. Physiol.* **585**, 263 (2007).
- [48] M. Coupland and K. W. Ranatunga, *J. Physiol.* **548**, 439 (2003).
- [49] R. C. Woledge, C. J. Barclay, and N. A. Curtin, *P Roy. Soc. Lond. B Bio.* **276**, 2685 (2009).
- [50] M. Linari and R. C. Woledge, *J. Physiol.* **487**, 699 (1995).
- [51] C. Veigel, M. Bartoo, D. White, J. Sparrow, and J. Moll, *Biophys. J.* **75**, 1424 (1998).
- [52] M. Tyska and D. Warshaw, *Cell Motil. Cytoskel.* **51**, 1 (2002).
- [53] E. Brunello, M. Caremani, L. Melli, M. Linari, M. Fernandez-Martinez, T. Narayanan, M. Irving, G. Piazzesi, V. Lombardi, and M. Reconditi, *The Journal of physiology* **592**, 3881 (2014).
- [54] N. van Kampen, *Stochastic Processes in Physics and Chemistry* (North-Holland, Amsterdam, 2001).
- [55] J.-D. Wen, M. Manos, P. T. X. Li, S. B. Smith, C. Bustamante, F. Ritort, and I. Tinoco, *Biophys. J.* **92**, 2996 (2007).
- [56] R. Podolsky, *Nature* **188**, 666 (1960).
- [57] M. Civan and R. Podolsky, *J. Physiol.* **184**, 511 (1966).
- [58] R. Podolsky, A. C. Nolan, and S. A. Zaveler, *Proc. Natl. Acad. Sci. U.S.A.* **64**, 504 (1969).
- [59] A. F. Huxley and R. M. Simmons, *J. Physiol.* **208**, 52P (1970).
- [60] K. Holmes and M. Geeves, *Philos. T. Roy. Soc. B* **355**, 419 (2000).
- [61] I. Rayment, H. Holden, M. Whittaker, C. Yohn, M. Lorenz, K. Holmes, and R. Milligan, *Science* **261**, 58 (1993).
- [62] R. Dominguez, Y. Freyzon, K. M. Trybus, and C. Cohen, *Cell* **94**, 559 (1998).
- [63] R. Lymn and E. Taylor, *Biochemistry* **10**, 4617 (1971).
- [64] B. Alberts, A. Johnson, J. Lewis, M. Raff, K. Roberts, and P. Walter, *Molecular Biology of the Cell*, 5th ed. (Garland Science, New York, 2007).
- [65] L. Hilbert, S. Kumarasamy, N. B. Zitouni, M. C. Mackey, and A.-M. Lauzon, *Biophysj* **105**, 1466 (2013).
- [66] L. Hilbert, Z. Balassy, N. B. Zitouni, M. C. Mackey, and A.-M. Lauzon, *Biophys. J.* **108**, 622 (2015).
- [67] J. E. Baker, C. Brosseau, P. B. Joel, and D. M. Warshaw, *Biophysj* **82**, 2134 (2002).
- [68] J. E. Baker, C. Brosseau, P. Fagnant, and D. M. Warshaw, *J. Biol. Chem.* **278**, 28533 (2003).
- [69] B. D. Haldeman, R. K. Brizendine, K. C. Facemyer, J. E. Baker, and C. R. Cremo, *J. Biol. Chem.* **289**, 21055 (2014).
- [70] Anneka M Hooft, Erik J Maki, K. K. Cox, and J. E. Baker, *Biochemistry* **46**, 3513 (2007).
- [71] J. Del R Jackson and J. E. Baker, *Physical Chemistry Chemical Physics* **11**, 4808 (2009).
- [72] M. Caremani, L. Melli, M. Dolfi, V. Lombardi, and M. Linari, *J. Physiol.* **593**, 3313 (2015).
- [73] S. H. Gilbert and L. E. Ford, *Biophysj* **54**, 611 (1988).
- [74] E. Pate, G. J. Wilson, M. Bhimani, and R. Cooke, *Biophysj* **66**, 1554 (1994).
- [75] M. Linari, R. Bottinelli, M. Pellegrino, M. Reconditi, C. Reggiani, and V. Lombardi, *J. Physiol. - London* **555**, 851 (2004).
- [76] K. W. Ranatunga, *The Journal of physiology* **588**, 3657 (2010).
- [77] M. Reconditi, *Rep. Prog. Phys.* **69**, 2709 (2006).
- [78] R. Sheshka and L. Truskinovsky, *Phys. Rev. E* **89**, 012708 (2014).
- [79] A. F. Huxley, *J. Physiol.* **243**, 1 (1974).
- [80] C. F. Armstrong, A. F. Huxley, and F. J. Julian, *J. Physiol.* **186**, 22P (1966).
- [81] K. A. P. Edman, *J. Physiol. - London* **404**, 301 (1988).
- [82] K. Yasuda, Y. Shindo, and S. Ishiwata, *Biophys. J.* **70**, 1823 (1996).
- [83] K. A. P. Edman and N. Curtin, *J. Physiol. - London* **534**, 553 (2001).
- [84] P. Y. Plaçais, M. Balland, T. Guerin, J. F. Joanny, and P. Martin, *Phys. Rev. Lett.* **103** (2009).
- [85] T. A. J. Duke, *Proc. Natl. Acad. Sci. USA* **96**, 2770 (1999).
- [86] T. Duke, *Philos. T. Roy. Soc. B* **355**, 529 (2000).
- [87] M. Badoual, F. Jülicher, and J. Prost, *Proc. Natl. Acad. Sci. U.S.A.* **99**, 6696 (2002).
- [88] S. Walcott and S. X. Sun, *Physical Chemistry Chemical Physics* **11**, 4871 (2009).
- [89] T. A. Duke, N. Le Novère, and D. Bray, *J. Mol. Biol.* **308**, 541 (2001).
- [90] D. Bray, *Journal of Molecular Biology* **425**, 1410 (2013).
- [91] V. Bormuth, J. Barral, J. F. Joanny, F. Jülicher, and P. Martin, *Proc. Natl. Acad. Sci. U.S.A.* **111**, 7185 (2014).
- [92] B. Chen and H. Gao, *Biophys. J.* **101**, 396 (2011).
- [93] H. Yao and H. Gao, *J. Mech. Phys. Solids* **54**, 1120 (2006).
- [94] H. Gao, J. Qian, and B. Chen, *J. R. Soc. Interface* **8**, 1217 (2011).
- [95] U. S. Schwarz and S. A. Safran, *Reviews of Modern Physics* **85**, 1327 (2013).
- [96] P. Hanggi, P. Talkner, and M. Borkovec, *Reviews of Modern Physics* **62**, 251 (1990).
- [97] T. Erdmann and U. S. Schwarz, *Phys. Rev. Lett.* **92**, 108102 (2004).
- [98] T. Erdmann and U. S. Schwarz, *J. Chem. Phys.* **121**, 8997 (2004).

- [99] U. Seifert, Phys. Rev. Lett. **84**, 2750 (2000).
- [100] T. C. Südhof and J. E. Rothman, Science **323**, 474 (2009).
- [101] D. Min, K. Kim, C. Hyeon, Y. H. Cho, Y.-K. Shin, and T.-Y. Yoon, Nat. Commun. **4**, 1705 (2013).
- [102] F. Li, F. Pincet, E. Perez, W. S. Eng, T. J. Melia, J. E. Rothman, and D. Tareste, Nature Structural & Molecular Biology **14**, 890 (2007).
- [103] S. Zorman, A. A. Rebane, L. Ma, G. Yang, M. A. Molski, J. Coleman, F. Pincet, J. E. Rothman, and Y. Zhang, Elife **3**, e03348 (2014).
- [104] H. Dietz and M. Rief, Phys. Rev. Lett. **100**, 098101 (2008).
- [105] R. Cerf, Proc. Natl. Acad. Sci. U.S.A. **75**, 2755 (1978).
- [106] E. Pfitzner, C. Wachauf, F. Kilchherr, and B. Pelz, Angew. Chem. Int. Ed. **52**, 335 (2013).
- [107] J. P. Changeux, J. Thiéry, Y. Tung, and C. Kittel, Proc. Natl. Acad. Sci. USA **57**, 335 (1967).
- [108] D. Bray and T. Duke, Annu Rev Biophys Biomol Struct **33**, 53 (2004).
- [109] B. M. Slepchenko and M. Terasaki, Current Opinion in Genetics & Development **14**, 428 (2004).
- [110] O. Miyashita, J. N. Onuchic, and P. G. Wolynes, PNAS **100**, 12570 (2011).
- [111] B. Yurke, A. J. Turberfield, A. P. Mills, F. C. Simmel, and J. L. Neumann, Nature **406**, 605 (2000).
- [112] R. L. Harne, Z. Wu, and K. W. Wang, J. Mech. Des **138**, 021402 (2016).
- [113] T. Guerin, J. Prost, and J. F. Joanny, Eur. Phys. J. **34**, 60 (2011).
- [114] Sheshka, R, Recho, P, and Truskinovsky, Lev, Phys. Rev. E **93**, 052604 (2016).